# Influence of wollastonite on hydration and properties of magnesium potassium phosphate cements

Biwan Xu[a*], Barbara Lothenbach[a,b], Frank Winnefeld[a]

[a]: Laboratory for Concrete & Construction Chemistry, Swiss Federal Laboratories for Materials Science and Technology (Empa), 8600 Dübendorf, Switzerland

[b]: Department of Structural Engineering, Norwegian University of Science and Technology, Trondheim, Norway

* Corresponding author: Biwan Xu; E-mail: biwan.xu@empa.ch or biwan.xu@outlook.com

**Abstract:** This study investigates the effect of wollastonite on the hydration and properties of magnesium potassium phosphate (MKP) cements. In MKP cements some efflorescence can occur; the presence of wollastonite suppresses efflorescence as the formation of $Mg_2KH(PO_4)_2 \cdot 15H_2O$ is prevented. The presence of wollastonite leads also to more heat (per g of MKP cement) due to the filler effect and due to the reaction of wollastonite, which increases strength, especially at low water-to-binder (w/b) ratio of 0.25 and at later ages, and lowers the pH values in the cement pore solution. The reaction of wollastonite does not lead to the formation of crystalline hydrates, both experimental and thermodynamic findings suggest the formation of amorphous hydroxyapatite and magnesium silicate hydrates (M-S-H).

Keywords: Magnesium potassium phosphate (MKP) cement; Wollastonite; Reactivity; Hydration; Strength.

## 1. Introduction

Magnesium potassium phosphate (MKP) cements, which harden through an acid-base reaction between calcined magnesia (MgO) and potassium dihydrogen phosphate ($KH_2PO_4$), is an alternative to Portland cement (PC). Compared to PC, MKP cements have the advantage of fast setting [1, 2], high early strength [3], low shrinkage [2], strong bonding with PC substrates [2], low pH [4-6], strong encapsulation capacity on heavy metals [7, 8], and good biocompatibility [9, 10]. They are used for various applications, such as rapid repair materials for damaged infrastructure [2, 11, 12], as solidification/stabilization agents for wastes containing heavy metals [1, 7, 8], and as potential binders for immobilizing low-level nuclear wastes [13-15]. Recent research involved also their use in medical technology due to their good biocompatibility and antibacterial properties [9, 10].

The hydration reaction of MKP cements can be changed by using different magnesium-to-phosphate ($Mg/PO_4$) molar ratios [6, 16], water-to-cement (w/c) ratios [4-6, 16], retarders [4], and mineral additions [14, 17, 18]. The dominant hardening reaction of MKP cements is described as

$$MgO + KH_2PO_4 + 5H_2O \rightarrow MgKPO_4{\cdot}6H_2O \text{ (K-struvite)} + Q_{Heat} \quad (1)$$

As shown in Eq. 1, magnesium potassium phosphate hexahydrate ($MgKPO_4{\cdot}6H_2O$, K-struvite) is the stoichiometric reaction product of hydrated MKP cements providing strength. Furthermore, hydration of MKP cements is exothermic with strong heat release ($Q_{Heat}$), which not only accelerates cement hardening, but also makes cement applications in large scales difficult [1, 19]. To slow down cement hydration kinetics and to control heat release, different methods have been used, such as i) use of retarders like borax [2] and boric acid [4, 14], ii) decrease of magnesia reactivity [20], iii) increase of initial pH by partially replacing $KH_2PO_4$ with $K_2HPO_4$ or

23 $Na_2HPO_4 \cdot 12H_2O$ [21, 22], and iv) cement dilution using mineral additions, such as fly ash [3, 14,
24 15, 17], silica fume [23, 24], metakaolin [18], and wollastonite [1, 25, 26].

25 Wollastonite ($CaSiO_3$) is an inosilicate mineral and has been used in cementitious materials for
26 decades [27-30]. It has microfiber-like particles, which effectively increased flexural strength and
27 fracture toughness of PC-based materials due to an enhanced crack resistance [27, 28]. However,
28 wollastonite shows no or only little reaction in PC matrices [27, 28], which is probably due to the
29 high pH of pore solution of around 13 – 14 [31], where wollastonite is more stable than C-S-H and
30 thus not reactive. At low pH wollastonite is better soluble and can release calcium and silicate ions.
31 Therefore, wollastonite has been used as raw material for producing low pH cements, such as
32 inorganic phosphate cements (ceramics) [32-35], carbonated wollastonite-based materials [30, 36],
33 and MKP cements [1, 25, 26]. The blend of wollastonite with MKP cements was reported to reduce
34 heat generation [1], to increase mechanical strength [1], and to improve heat resistance under high
35 temperatures [25]. Moreover, it has been assumed that wollastonite reacts with potassium and
36 phosphate from the MKP cements and leads to formation of brushite ($CaHPO_4 \cdot 2H_2O$) and
37 potassium metasilicate ($K_2SiO_3$) [1, 26]; however, experimental evidence is missing.

38 As only limited information regarding the reactivity of wollastonite and the resultant additional
39 hydrates are available, this study investigates the effect of wollastonite (i) on the strength of MKP
40 cements at low water-to-binder (w/b) ratios of 0.25 and 0.5, and (ii) on the hydration at w/b ratios
41 of 0.5 and 5, which were characterized by isothermal calorimetry and determination of cement
42 hydrate assemblage and pore solution chemistry.
43
44
45

## 2. Materials and methods

### 2.1 Materials and mix designs

The starting materials included dead-burnt magnesia (MgO), wollastonite ($CaSiO_3$), quartz powder, and $KH_2PO_4$ in technical grades, and magnesium chloride ($MgCl_2$) in chemical grade. Chemical compositions of magnesia, wollastonite and $KH_2PO_4$ determined by X-ray florescence (XRF) analysis are given in Table 1. Mineralogical composition of magnesia and wollastonite was determined by X-ray diffraction method (XRD, CoKα, Panalytical X'Pert Pro). Magnesia contains a main phase of periclase (MgO) and minor impurities of forsterite ($Mg_2SiO_4$) and monticellite ($CaMgSiO_4$). Wollastonite contains a main phase of 'wollastonite-2M' ($CaSiO_3$) and traces of quartz ($SiO_2$) and calcite ($CaCO_3$). The characterization using secondary electron microscopy (SEM, ESEM Quanta FEG 650) shows a microfiber-like shape of most wollastonite particles. The median particle diameters ($d_{50}$) of magnesia, wollastonite and $KH_2PO_4$ measured by a laser particle size analyzer (Malvern Mastersizer X) are 19.0 ± 0.3, 3.7 ± 0.5, and 34.4 ± 4.8 μm, respectively.

Table 1: Chemical composition of raw materials wt.%

| Materials | MgO | $SiO_2$ | $Al_2O_3$ | $Fe_2O_3$ | CaO | $K_2O$ | $Na_2O$ | $TiO_2$ | $SO_3$ | $P_2O_5$ | $CO_2$[a] | L.O.I[b] |
|---|---|---|---|---|---|---|---|---|---|---|---|---|
| Magnesia | 93.54 | 4.37 | 0.04 | 0.15 | 1.62 | <0.02 | <0.04 | <0.007 | <0.04 | 0.008 | 0.18 | 0.18 |
| Wollastonite | 0.41 | 51.86 | 0.86 | 0.19 | 44.15 | 0.12 | 0.31 | 0.019 | 0.05 | 0.009 | 0.50 | 1.99 |
| $KH_2PO_4$ | 0.45 | 2.01 | <0.3 | 0.007 | <0.06 | 36.63 | 0.28 | 0.02 | <0.024 | 40.44 | n.d.[c] | 20.94 |

[a]: $CO_2$ content was calculated based on the total carbon content determined by combustion analyses.
[b]: Loss on ignition. [c]: not detected.

Mix proportions used in this study are present in Table 2. Three systems were studied: A) cement pastes with a $Mg/PO_4$ molar ratio of 2.7 and w/b ratios in a range of 0.25 – 0.83; B) cement suspension with the same $Mg/PO_4$ molar ratio of 2.7 and w/b ratio of 5, and C) suspensions of wollastonite blended with $KH_2PO_4$, magnesia or $MgCl_2$, which have w/b ratios of 5.2 and 6.8. All

the samples were cured at 20 °C, except the suspensions of wollastonite mixed with magnesia (W-MgO-S) or $MgCl_2$ (W-MgCl-S) at 50 °C.

Table 2: Mix proportions of wollastonite-magnesium-phosphate systems referred to 1 g $KH_2PO_4$

| Sample | $Mg/PO_4$ ratio[a] | w/b[b] ratio | w/c[b] ratio | Wollastonite | $KH_2PO_4$ | Magnesia | $MgCl_2$ | Quartz powder | Water | $t_{FS}$ [min] |
|---|---|---|---|---|---|---|---|---|---|---|
| ***A): MKP cement pastes*** | | | | | | | | | | |
| **2.7-C-P025[c]** | 2.7 | 0.25 | 0.25 | - | 1.0 | 0.8 | - | - | 0.45 | 11 ± 2 |
| **2.7-W-P025[c]** | 2.7 | 0.25 | 0.42 | 1.2 | 1.0 | 0.8 | - | - | 0.75 | 36 ± 5 |
| **2.7-C-P05[d]** | 2.7 | 0.5 | 0.5 | - | 1.0 | 0.8 | - | - | 0.9 | - |
| **2.7-W-P05[d]** | 2.7 | 0.5 | 0.83 | 1.2 | 1.0 | 0.8 | - | - | 1.5 | - |
| **2.7-Q-P05[e]** | 2.7 | 0.5 | 0.83 | - | 1.0 | 0.8 | - | 1.2 | 1.5 | - |
| **2.7-C-P08[e]** | 2.7 | 0.83 | 0.83 | - | 1.0 | 0.8 | - | - | 1.5 | - |
| ***B): MKP cement suspensions*** | | | | | | | | | | |
| **2.7-C-S5[f]** | 2.7 | 5.0 | 5.0 | - | 1.0 | 0.8 | - | - | 9.0 | - |
| **2.7-W-S5[f]** | 2.7 | 5.0 | 8.3 | 1.2 | 1.0 | 0.8 | - | - | 15.0 | - |
| ***C): Wollastonite - $KH_2PO_4$ ($MgO$ / $MgCl_2$) suspensions*** | | | | | | | | | | |
| **W-K-S[g]** | - | 6.8 | - | 1.2 | 1.0 | - | - | - | 15.0 | - |
| **W-MgO-S[g]** | - | 6.8 | - | 1.2 | - | 2.4 | - | - | 24.5 | - |
| **W-MgCl-S[g]** | - | 5.2 | - | 1.2 | - | - | 1.4 | - | 13.6 | - |

[a]: molar ratio. [b]: w/b denotes water-to binder mass ratio. For MKP cement systems, binder refers to sum of magnesia, $KH_2PO_4$, and wollastonite (quartz). w/c denotes water-to-cement ratio, and cement refers to sum of magnesia and $KH_2PO_4$. For wollastonite- $KH_2PO_4$ ($MgO$/$MgCl_2$) suspension, binder refers to sum of wollastonite and $KH_2PO_4$ (magnesia or $MgCl_2$). [c]: analyses of final setting time ($t_{FS}$), compressive and flexural strength. Final setting time was measured by Vicat needle test using fresh paste around 200 g. [d]: analyses of calorimetry and determination of hydrate assemblage and pore solution chemistry. Also, compressive and flexural strength of 2.7-W-P05 was determined. [e]: calorimetry only. [f]: analyses of calorimetry, pH/electrical conductivity, and determinations of hydrate assemblages and pore solution chemistry. [g]: determination of hydrate assemblages. Mass ratio between wollastonite and $KH_2PO_4$ of W-K-S was kept consistent with that of 2.7-W-S5. W-K-S was cured at 20 °C up to 340 days. Ratios between $KH_2PO_4$ and magnesia (W-MgO-S) or $MgCl_2$ (W-MgCl-S) were used to guarantee sufficient magnesium source in water. To accelerate potential chemical reactions, they were cured at 50 °C for 110 and 180 days, respectively.

## 2.2 Methods

### 2.2.1 Compressive and flexural strength

According to the mix proportions given in Table 2, the powder components of the samples (2.7-C-P025, 2.7-W-P025, and 2.7-W-P05) were weighted and well dry-mixed for 1 min. After that, deionized water was added and wet-mixing using a vacuum mixer was carried out at a speed of 250 rpm for 2 min. Fresh mixtures were cast in molds with dimensions of $20 \times 20 \times 100$ mm$^3$. All the samples were cured in air at 20 °C and relative humidity (RH) of 70% until strength test after 3, 7, 28, 72, 200, 690, and 850 days. A three-point bending test was carried out first using a span of 60 mm at a loading rate of 20 N/s. Two prisms were measured for each paste after each specific curing age. After that, the obtained four prism halves were used for compressive strength measurement at a loading rate of 1 MPa/s using a contact surface area of $20 \times 20$ mm$^2$.

### 2.2.2 Isothermal calorimetry

As specified in Table 2, heat flow of the cement pastes with w/b ratios of 0.5 and 0.83 were measured using isothermal conduction calorimetry (TA instrument, TAM Air) at 20 °C. Powder components were weighted into Admix ampoule and well dry-mixed for 1 min. After thermal equilibration, deionized water was injected into Admix ampoule, and the mixture was wet-mixed for 2 min. Note that segregation could occur in samples at high w/b ratio.

### 2.2.3 X-ray diffraction and thermogravimetric analyses

To analyze hydrate assemblage, cement hydration was stopped after specific curing ages. Suspension samples were filtered using a Büchner funnel under vacuum. The remaining solids were soaked in isopropanol for around 15 min. Afterwards isopropanol was removed by filtration,

and diethyl ether was used to rinse the solids and removed by filtration as well. The solids were then dried at 40 °C for around 10 min to remove any remaining organic solvents, and stored in sealed bottles. Paste samples were gently crushed into small pieces first, and the same hydration stoppage protocol was then applied. The stopped samples were further ground by hand to a grain size less than 63 μm before XRD and thermogravimetric analysis (TGA). XRD analyses were performed with a Panalytical X'pert Pro in a Θ-Θ configuration using CoKα radiation and the X'Celerator detector. The samples were scanned between 5° and 90° 2θ for 45 min. Wollastonite and magnesia consumptions in hydrated samples were assessed semi-quantitatively by fitting peak areas in X'Pert Highscore Plus software using $CaF_2$ as an external standard for the intensity correction. Reaction degrees of magnesia (2.7-C-P05 and 2.7-W-P05 after 28 days) and wollastonite (2.7-W-P05 from 5 h to 420 days) were estimated by comparing the corrected peak intensities between unhydrated and hydrated samples. In consideration of fast dissolution of $KH_2PO_4$ at high w/b ratio of 5, reaction degree of wollastonite in 2.7-W-S5 from 22 min to 150 days were estimated by comparing the corrected peak intensities between the sample after 5 min of hydration and the rest hydrated samples. After quantification, all the results were further corrected according to [37] for bound water based on TGA result at 600 °C. TGA was carried out using Mettler Toledo TGA/SDTA 815e device from 30 to 1000 °C at heating rate of 20 °C/min under nitrogen atmosphere.

### 2.2.4 Nuclear magnetic resonance (NMR) analysis

Solid-state nuclear magnetic resonance (NMR) spectra of K-struvite [16], potassium calcium hydrogen phosphate ($CaK_3H(PO_4)_2$) [6], unhydrated cement with wollastonite (2.7-W-P05), and hydrated cements (2.7-C-P05, 2.7-W-P05, and 2.7-W-S5) were collected on a Bruker AV III HD

400 MHz widebore spectrometer. $^{29}Si$ MAS NMR spectra were collected using a probe of 7 mm, at 79.505 MHz at a spinning speed of 4.5 KHz with a plus duration of 2.5 μs. $^{31}P$ MAS NMR spectra were collected using a probe of 2.5 mm, at 161.995 MHz at a spinning speed of 20 KHz with a plus duration of 2.5 μs. $^{29}Si$ and $^{31}P$ chemical shifts are referenced to external samples of tetramethylsilane ($Si(CH_3)_4$) and ammonium dihydrogen phosphate ($NH_4H_2PO_4$), respectively.

### 2.2.5 Scanning electron microscopy (SEM)

Backscattered electron (BSE) imaging coupled with energy dispersive X-ray spectroscopy (EDS) analysis was carried out on cement polished sections. Hydration stoppage protocol for cement suspension as described above was applied to 2.7-W-S5 after 150 days. The stopped powder sample was first mixed with a low-viscosity epoxy resin; after that, the hardened resin was cut, polished, coated with 10 nm carbon. For 2.7-W-P05, paste sample with a diameter of 20 mm and a height of 15 mm after 420 days was cut from center of a cylinder, and soaked in isopropanol for one week first and dried in oven at 40 °C for two weeks. After that, it was impregnated with the same low-viscosity epoxy resin and applied with the same procedures for cutting, polishing and carbon coating. The conduction of SEM was under high vacuum mode ($3 - 4 \times 10^{-6}$ Pa) with an accelerating voltage of 10 – 15 kV.

### 2.2.6 Electrical conductivity and pH

The changes of electrical conductivity and pH in hydrated cement suspensions (2.7-C-S5 and 2.7-W-S5) were monitored in real time using the setup detailed in [16]. The pH electrode (Mettler Toledo) was calibrated against pH buffers at pH 4, 7, 9, and 12 before each measurement. As detailed in [16], cement suspension was filled in a vessel with a lid tightly locked to avoid possible

159 carbonation and water evaporation. A water bath at 20 °C was used to ensure a stable thermal
160 condition during test. Cement suspension was continuously stirred by an overhead stirrer. The
161 measured data was automatically recorded at time steps of 1 min.

162 2.2.7 Ion activities and elemental concentrations

163 $K^+$- and $Mg^{2+}$- selective electrodes and the setup presented above for the electrical conductivity
164 and pH measurement were used to measure $K^+$ and $Mg^{2+}$ activities in hydrated cement suspensions
165 (2.7-C-S5 and 2.7-W-S5). The $K^+$-selective electrode (perfectION$^{TM}$ comb K Lemo) was calibrated
166 against $KH_2PO_4$ standard solutions at 0.0044, 0.04, 0.22, 0.43, 0.48, and 0.77 M. Hydrate
167 precipitations on the surface of the $Mg^{2+}$-selective electrode (DX244-Mg) could affect the
168 measured value, therefore, measured raw data in mV instead of absolute concentrations are given
169 in this study.

170 Ion chromatography (IC, Dionex, DP series ICS-3000) was used to measure the total ion
171 concentrations in liquid phase of cements. Solution of the cement suspensions (2.7-C-S5 and 2.7-
172 W-S5) were obtained using a nylon filter with a mesh size of 0.45 μm. Pore solution of the hardened
173 cement pastes (2.7-C-P05 and 2.7-W-P05) were extracted from samples cast in 500 mL
174 polyethylene bottles (sealed curing at 20 °C) by the steel die method [31, 38], and filtered using
175 the same type of nylon filter. One part of the solution was diluted using Milli-Q water (ultra-pure
176 water) for IC measurement, and the other part was used undiluted for pH measurement (Meter 766).
177 The pH meter was calibrated against pH buffers at pH 4, 7, 9, and 12.

178

179 2.2.8 Thermodynamic modelling

180 The calculation of saturation indices from measured aqueous concentrations allows to assess
181 whether the pore solution is saturated with respect to different hydrates, which thus may precipitate

as discussed in detail e.g. in [39]. If the pore solution is oversaturated with respect to a certain solid, the solid is likely to precipitate; while undersaturation indicates that a solid is unlikely to precipitate or that it dissolves. The saturation index (SI) of a solid corresponds to SI = log IAP/$K_{so}$. The ion activity product (IAP) is calculated based on the measured concentrations in solution and $K_{so}$ represents the theoretical solubility product of the solid. As the use of saturation indices can be misleading when comparing phases which dissociate into a different number of ions, ''effective'' saturation indices were calculated where the saturation indices was divided by the number of ions participating in the reactions to form the solids [31, 39], i.e., the saturation indices for brucite, newberyite, phosphorrösslerite, K-struvite, $Mg_2KH(PO_4)_2 \cdot 15H_2O$, $Mg_3(PO_4)_2 \cdot 4H_2O$, bobierrite, cattiite, brushite, octacalcium phosphate, hydroxyapatite, and $CaK_3H(PO_4)_2$ are divided by 3, 3, 3, 3, 6, 5, 5, 5, 3, 16, 9, and 7. The formation from the ions $Mg^{2+}$, $Ca^{2+}$, $PO_4^{3-}$, $SiO_3^{2-}$, $K^+$, and $H^+$ was considered but not the influence of $H_2O$.

The geochemical GEMS-PSI software [40] together with the PSI thermodynamic database [41], the cement-specific Cemdata18 [42] and the recently complied database of magnesium (potassium) phosphates [43], extended with data for calcium phosphates and M-C-S-H [44], were used for the calculation as summarized in Table 3. The lower solubility of the calcium phosphate solids in Table 3 indicate an even higher stability of calcium phosphate than of Mg-phosphates solids and thus a tendency for the formation of calcium phosphates in the presence of calcium.

Table 3: Solubility products (log $K_{so}°$) of calcium, magnesium, phosphate and potassium containing solids at standard conditions 25 °C and 1 bar.

| Species | log $K_{so}°$[a] | Ref[b] |
|---|---|---|
| Brucite: $Mg(OH)_2 \Leftrightarrow Mg^{2+} - 2H^+$ | 16.84 | [41] |
| Newberyite: $MgHPO_4 \cdot 3H_2O \Leftrightarrow Mg^{2+} + H^+ + PO_4^{3-} + 3H_2O$ | -17.93 | [43] |
| Phosphorrösslerite: $MgHPO_4 \cdot 7H_2O \Leftrightarrow Mg^{2+} + H^+ + PO_4^{3-} + 7H_2O$ | -17.01 | [43] |

| | | | |
|---|---|---|---|
| K-struvite: $MgKPO_4 \cdot 6H_2O \Leftrightarrow Mg^{2+} + K^+ + PO_4^{3-} + 6H_2O$ | -10.96 | [43] |
| $Mg_2KH(PO_4)_2 \cdot 15H_2O \Leftrightarrow 2Mg^{2+} + K^+ + H^+ + 2PO_4^{3-} + 15H_2O$ | -28.67 | [43] |
| $Mg_3(PO_4)_2 \cdot 4H_2O \Leftrightarrow 3Mg^{2+} + 2PO_4^{3-} + 4H_2O$ | -23.50 | [43] |
| Bobierrite: $Mg_3(PO_4)_2 \cdot 8H_2O \Leftrightarrow 3Mg^{2+} + 2PO_4^{3-} + 8H_2O$ | -25.30 | [43] |
| Cattiite: $Mg_3(PO_4)_2 \cdot 22H_2O \Leftrightarrow 3Mg^{2+} + 2PO_4^{3-} + 22H_2O$ | -23.03 | [43] |
| Brushite: $CaHPO_4 \cdot 2H_2O \Leftrightarrow Ca^{2+} + H^+ + PO_4^{3-} + 2H_2O$ | -18.95 | [45] |
| Octacalcium phosphate: $Ca_8H_2(PO_4)_6 \cdot 5H_2O \Leftrightarrow 8Ca^{2+} + 2H^+ + 6PO_4^{3-} + 5H_2O$ | -96.80 | [46] |
| Hydroxyapatite: $Ca_5(PO_4)_3(OH) \Leftrightarrow 5Ca^{2+} + 3PO_4^{3-} + OH^-$ | -58.0 | [45, 47] |
| $CaK_3H(PO_4)_2 \Leftrightarrow Ca^{2+} + 3K^+ + H^+ + 2PO_4^{3-}$ | -22.4 | ts |
| | | |
| *C-S-H (CSHQ solid solution):* | | |
| $(CaO)_{0.67}SiO_2(H_2O)_{1.5}$: $^2/_3Ca^{2+} + SiO(OH)_3^- + {}^1/_3OH^- - {}^1/_6H_2O$ | -6.19 | [40, 42] |
| $(CaO)_{0.83}(SiO_2)_{0.67}(H_2O)_{1.83}$: $^5/_6Ca^{2+} + {}^2/_3SiO(OH)_3^- + OH^- + {}^1/_3H_2O$ | -6.90 | [40, 42] |
| $(CaO)_{1.33}SiO_2(H_2O)_{2.17}$: $^4/_3Ca^{2+} + SiO(OH)_3^- + {}^5/_3OH^- - {}^1/_6H_2O$ | -10.96 | [40, 42] |
| $(CaO)_{1.5}(SiO_2)_{0.67}(H_2O)_{2.5}$: $^3/_2Ca^{2+} + {}^2/_3SiO(OH)_3^- + {}^7/_3OH^- + {}^1/_3H_2O$ | -10.47 | [40, 42] |
| | | |
| *M-S-H (M-C-S-H solid solution):* | | |
| $(MgO)_{0.78}SiO_2(H_2O)_{1.48} \rightarrow 0.78Mg^{2+} + SiO_2^0 + 1.56OH^- + 0.7H_2O$ | -14.59 | [40, 42] |
| $(MgO)_{0.68}(CaO)_{0.1}SiO_2(H_2O)_{1.48} \rightarrow 0.68Mg^{2+} + 0.1Ca^{2+} + SiO_2^0 + 1.56OH^- + 0.7H_2O$ | -14.42 | [40, 42] |
| $(MgO)_{1.3}SiO_2(H_2O)_{1.8} \rightarrow 1.3Mg^{2+} + SiO_2^0 + 2.6OH^- + 0.5H_2O$ | -21.44 | [44] |
| $(MgO)_{1.2}(CaO)_{0.1}SiO_2(H_2O)_{1.8} \rightarrow 1.2Mg^{2+} + 0.1Ca^{2+} + SiO_2^0 + 2.6OH^- + 0.5H_2O$ | -21.57 | [44] |

[a] The presence of aqueous phosphate complexes were considered using the data compiled in [43] completed with data for calcium phosphate complexes from [46]. [b] ts: calculated in this study, see appendix A.

## 3 Results and discussion

### 3.1 Cement pastes

#### 3.1.1 Segregation and strength development

The appearances of the MKP cement paste samples with/without wollastonite at w/b ratios of 0.25 and 0.5 are displayed in Figure 1. The reference paste samples without wollastonite (2.7-C-P05 and 2.7-C-P025) show clear segregations, especially at w/b of 0.5. At high w/b ratio magnesia particles preferably segregate due to the higher density compared to $KH_2PO_4$, which leads to a higher w/b ratio and a lower $Mg/PO_4$ molar ratio at the upper part of the sample causing the formation of efflorescence [6]. The partial replacement of cement with wollastonite prevents the segregation as well as the efflorescence, which is attributed to the smaller particle size of wollastonite and/or potential chemical reactions occurring during setting and hardening. As indicated in Table 2, the paste with wollastonite at w/b ratio of 0.25 (2.7-W-P025) has longer final setting time than the reference paste without wollastonite (2.7-C-P025), which is probably due to the dilution of the cement by wollastonite.

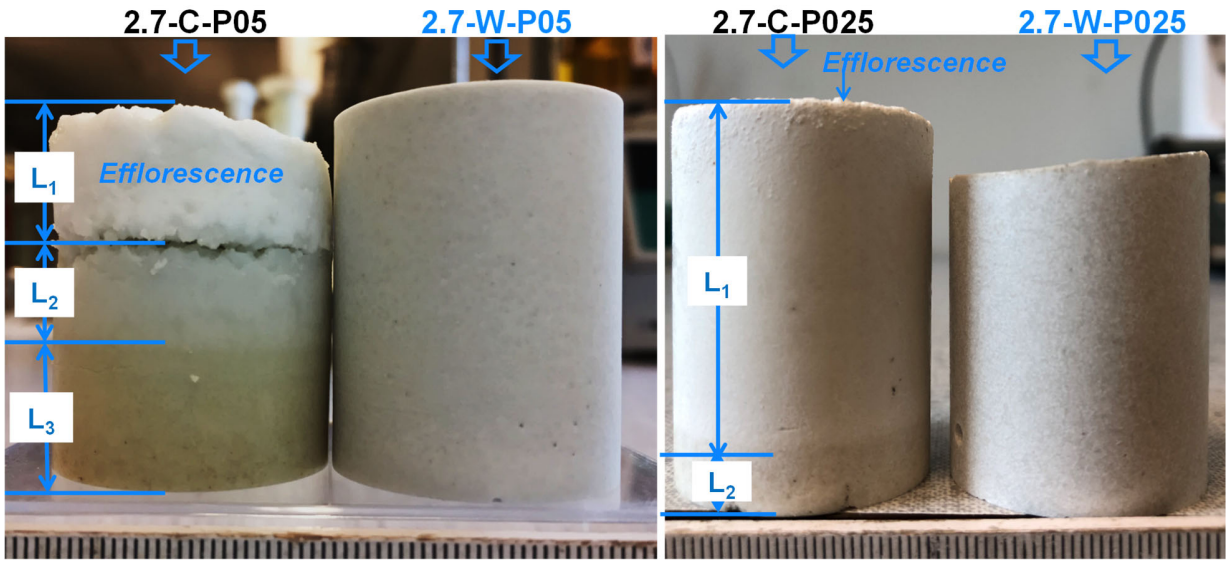


Figure 1: Appearances of the samples with/without wollastonite at w/b ratios of 0.25 and 0.5

253 Figure 2 shows the strength developments of the pastes at w/b ratios of 0.25 and 0.5. Strengths
254 of the reference paste without wollastonite at w/b ratio of 0.5 (2.7-C-P05) were not measured due
255 to the strong segregation as shown in Figure 1. As detailed in [6], strengths of 2.7-C-P025 increase
256 first up to 7 days and decrease thereafter due to volume expansion and resulting crack formations.
257 For the pastes with wollastonite, the decrease of w/b ratio from 0.5 to 0.25 strongly increases
258 compressive and flexural strengths. The strengths of the sample with wollastonite, 2.7-W-P025,
259 are up to 7 days lower than that of 2.7-C-P025, but much higher after 28 days and later. The
260 continuous strength increase of 2.7-W-P025 with time indicates a continuing condensed
261 microstructure.
262

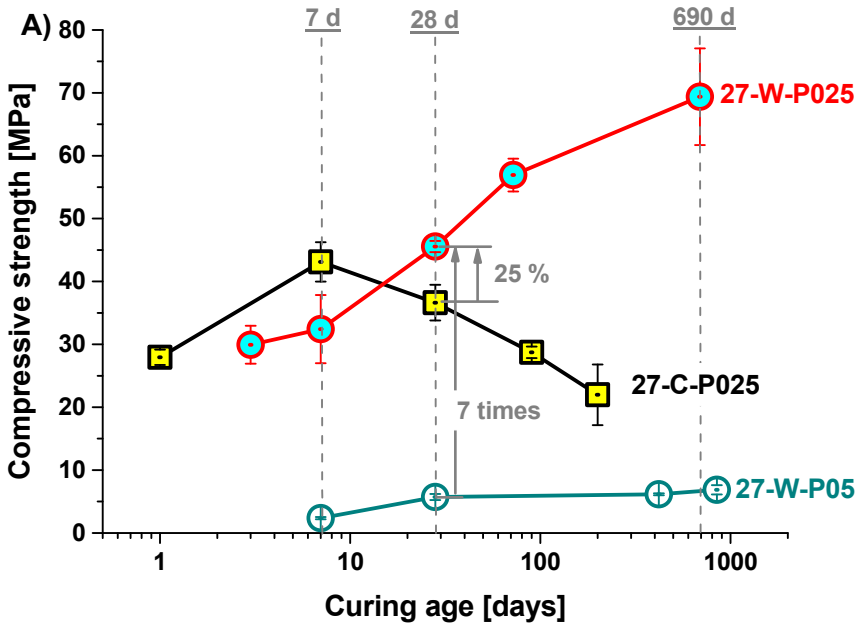


263

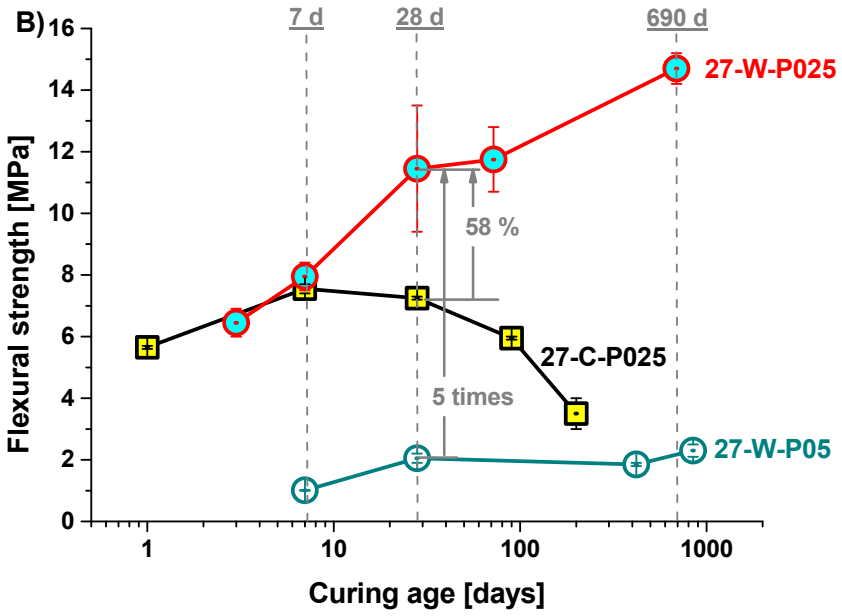


Figure 2: A) Compressive and B) flexural strengths of pastes with (2.7-W-P025, 2.7-W-P05) /without (2.7-C-P025) wollastonite at w/b ratios of 0.25 and 0.5. Strengths of the reference paste without wollastonite (2.7-C-P025) at w/b ratio of 0.25 were taken from [6].

### 3.1.2 Isothermal calorimetry

The results of isothermal calorimetry are shown in Figure 3. Quartz powder was used as a reference to distinguish between the effect of additional water and surface on cement hydration (filler effect) and the contribution of the reaction of wollastonite. As displayed in Figure 3A and B, the release of hydration heat is almost finished after 48 hours, and the main hydration reactions occur during the first 8 hours. During the first minutes endothermic heat events are observed for all pastes due to the dissolution of $KH_2PO_4$ in water, and the higher endothermic heat events of the pastes with wollastonite or quartz powder (2.7-W-P05 and 2.7-Q-P05) are due to their higher w/c ratio of 0.83 as given in Table 2. The first exothermic peak is comparable for all the pastes. The second exothermic peaks of 2.7-W-P05 and 2.7-Q-P05 show higher intensity and are shifted to

earlier hydration time as compared to the corresponding 2.7-C-P05. Moreover, 2.7-W-P05 shows the highest cumulative heat up to 48 hours, which can be partially attributed to the filler effect of wollastonite, similar to the filler effect of quartz powder in PC [48]. In fact, the higher cumulative heat per g cement of the reference paste with quartz (2.7-Q-P05) shows that the additional water and /or nucleation sites on the quartz surface enhance MKP reaction. The cumulative heat after 48 h of the sample (2.7-C-P08), which has the same w/c of 0.83 as the samples with quartz or wollastonite at w/b = 0.5, is somewhat lower (Figure 3B) as a higher fraction of potassium and phosphate remain in solution, indicating that the presence of additional nucleation sites on the quartz surface play an important role for the cement reaction. The higher total heat of the wollastonite containing sample (2.7-W-P05) indicates that wollastonite contributes to heat of hydration due to participation in the chemical reactions.

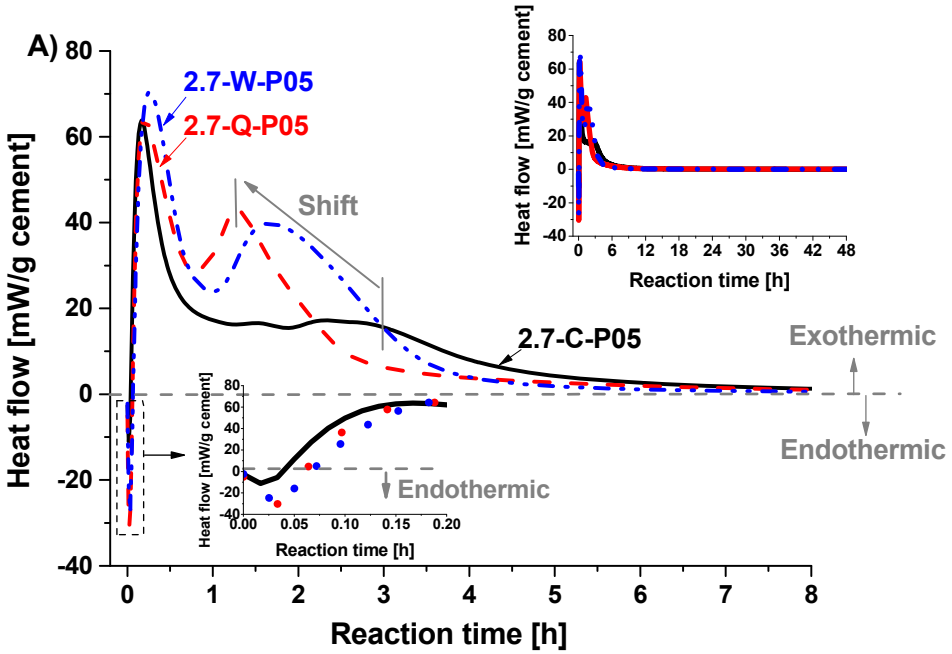

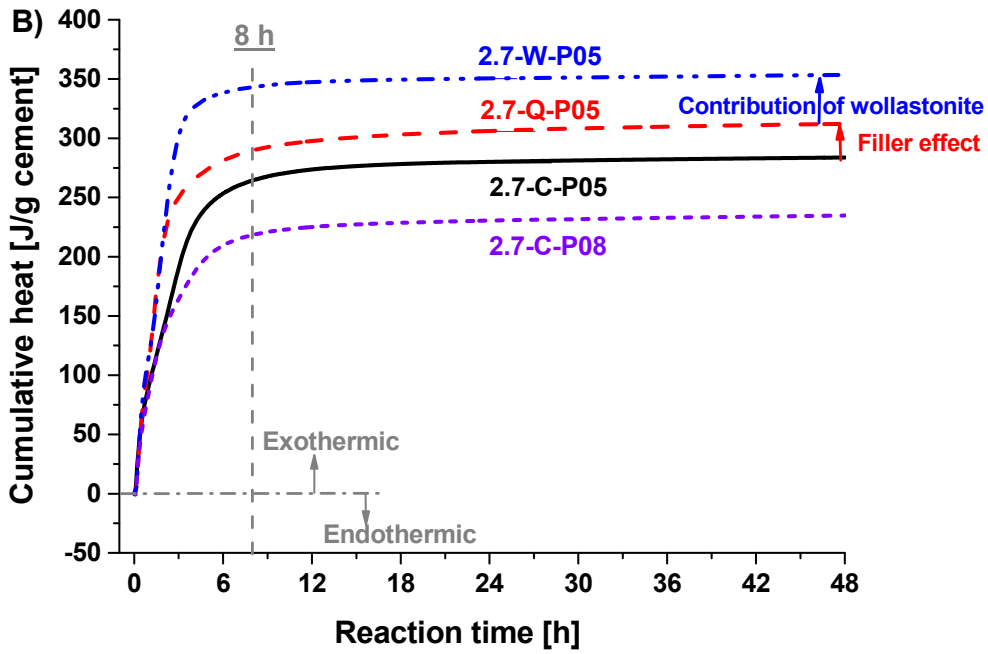


Figure 3: A) Heat flow, B) cumulative heat of the hydrated pastes (2.7-C-P05, 2.7-C-P08, 2.7-W-P05, and 2.7-Q-P05) after 48 hours. Results of the heat flow and cumulative heat are normalized to the weight of magnesia plus $KH_2PO_4$, which is referred to as 'cement' in the unit of the Y-axis.

### 3.1.3 Expected hydrate assemblage

Thermodynamic modelling using the thermodynamic data compiled in Table 3 was used to predict the effect of wollastonite reaction on a well-hydrated MKP cement with a $Mg/PO_4 = 2.7$. Figure 4 shows that in the absence of wollastonite, the MKP cement is calculated to obtain in addition unreacted MgO mainly K-struvite plus some $Mg_2KH(PO_4)_2 \cdot 15H_2O$ in agreement with experimental results presented in [6] and shown below. The reaction of wollastonite is calculated to destabilize initially $Mg_2KH(PO_4)_2 \cdot 15H_2O$ and then K-struvite to hydroxyapatite and M-(-C)-S-H (using a simplified M-S-H composition of $(MgO)_{0.6}SiO_2(H_2O)_{1.2}$) according to:

$$3MgKPO_4 \cdot 6H_2O + 5CaSiO_3 \Leftrightarrow Ca_5(PO_4)_3(OH) + 5M\text{-}S\text{-}H + 3K^+ + 3OH^- + 10H_2O \quad (2)$$

In addition, at very high wollastonite reaction degree of > 66%, a minor amount of $CaK_3H(PO_4)_2$ and some C-S-H are predicted; further $CaK_3H(PO_4)_2$ is fully destabilized to hydroxapatite at high reaction degree of around 85%.

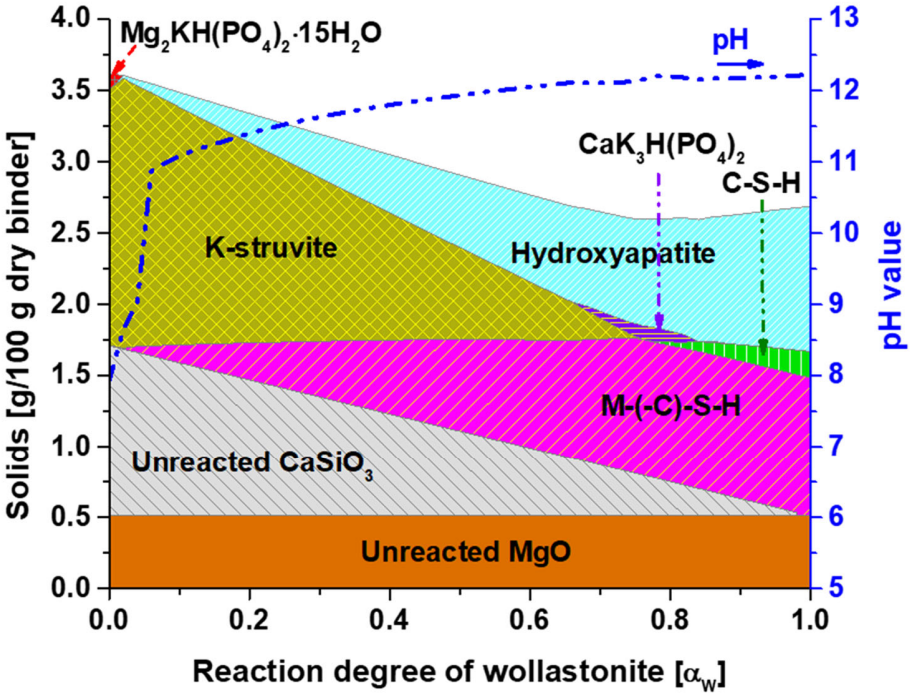


Figure 4: Calculated hydrate assemblage in 2.7-W-P05 as a function of wollastonite reaction degree ($\alpha_W$). The thermodynamic data compiled in Table 3 were used and a reaction degree of 36% for MgO was used according to the experimentally observed reaction degree of MgO (see below).

### 3.1.4 Experimentally observed hydrate assemblages

For the reference paste without wollastonite (2.7-C-P05), most $KH_2PO_4$ is consumed within the first day, leading to the formation of mainly K-struvite (see Figure 5A). Also, $Mg_2KH(PO_4)_2{\cdot}15H_2O$ and an unidentified phase with reflections at 11.9, 16.2, 26.3, 26.7, and 40.9°

319 2θ CoKα (d-spacing values: 8.6, 6.3, 3.9, 3.9, and 2.6 Å) are observed after 1 day and still present
320 after 28 days. $Mg_2KH(PO_4)_2 \cdot 15H_2O$ is destabilized to K-struvite at high w/b ratios, e.g. 5 or above
321 [4-6, 16], but persists at low w/b ratios, e.g. 0.25 or 0.5, and causes efflorescence [6] as also
322 observed for the reference samples in Figure 1. The observed hydrates agree well with calculations
323 in the absence of any wollastonite reaction shown in Figure 4.

324 For the paste with wollastonite (2.7-W-P05), a different hydration path is observed as shown in
325 Figure 5B. Compared to 2.7-C-P05, $KH_2PO_4$ is consumed faster and cannot be detected by XRD
326 after only 1 hour of hydration. Based on the results of XRD (Figure 5B) and TGA (Figure 6B), the
327 reaction degrees of wollastonite with time are estimated and shown in Figure 5C. After 5 hours of
328 hydration, the reaction degree of wollastonite is around 42%. The high early reaction degree of
329 wollastonite is related to the low pH values at early times, which accelerate the wollastonite
330 reaction; while at pH values above 8, little further wollastonite reaction is expected [49, 50]. This
331 fast reaction is consistent with the rapid heat release as shown in Figure 3. However, the reaction
332 degree shows little changes between 5 hours and 28 days. The dissolution of wollastonite further
333 slows down between 28 and 420 days, leading to a reaction degree of around 62% after 420 days.

334 K-struvite is the only crystalline hydrate throughout the entire investigated period. No
335 additional crystalline hydrates are observed although the reflection intensities of wollastonite are
336 reduced with time. This contradicts the findings reported by Wagh et al. [1, 26], who suggested the
337 formation of brushite ($CaHPO_4 \cdot 2H_2O$) and potassium metasilicate ($K_2SiO_3$) together with K-
338 struvite in MKP cements with wollastonite. The absence of additional hydrates from dissolution of
339 wollastonite indicates they could be either amorphous, in small amounts, or intermixed with K-
340 struvite, which is explored further in the following sections.

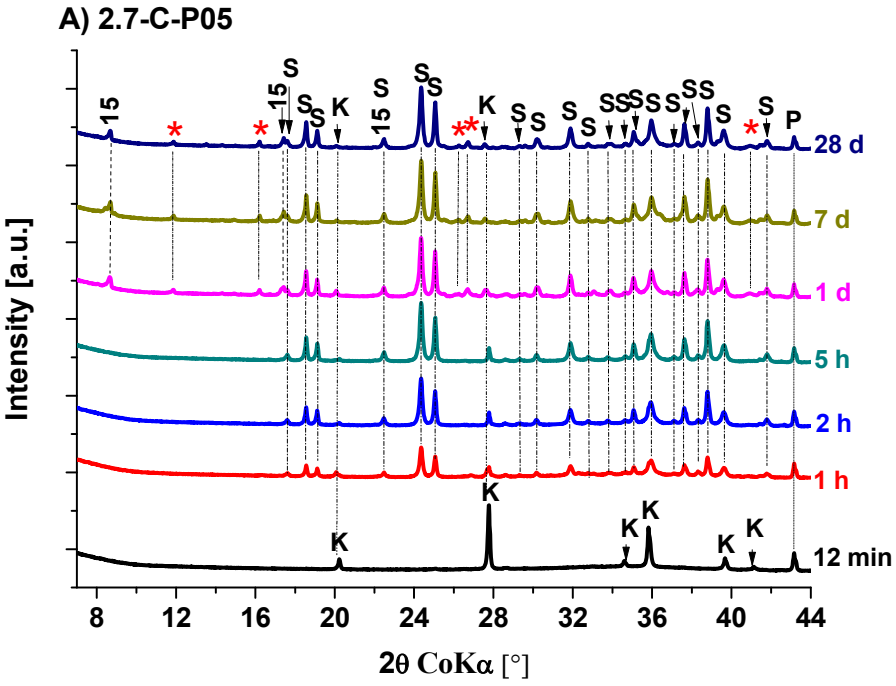
A) 2.7-C-P05
Intensity [a.u.]
28 d
7 d
1 d
5 h
2 h
1 h
12 min
8
12
16
20
24
28
32
36
40
44
2θ CoKα [°]

341

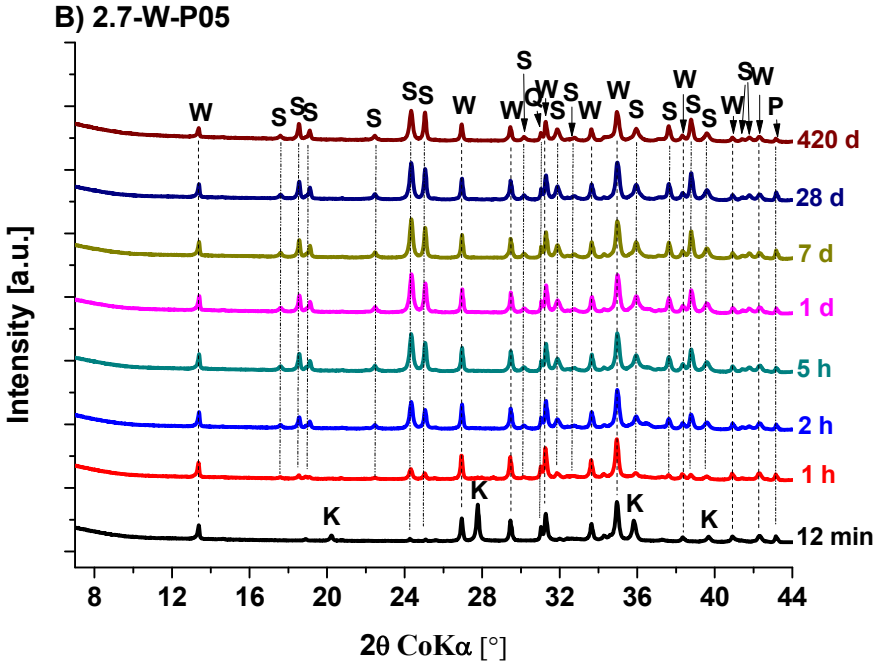
B) 2.7-W-P05
Intensity [a.u.]
420 d
28 d
7 d
1 d
5 h
2 h
1 h
12 min
8
12
16
20
24
28
32
36
40
44
2θ CoKα [°]

342

343

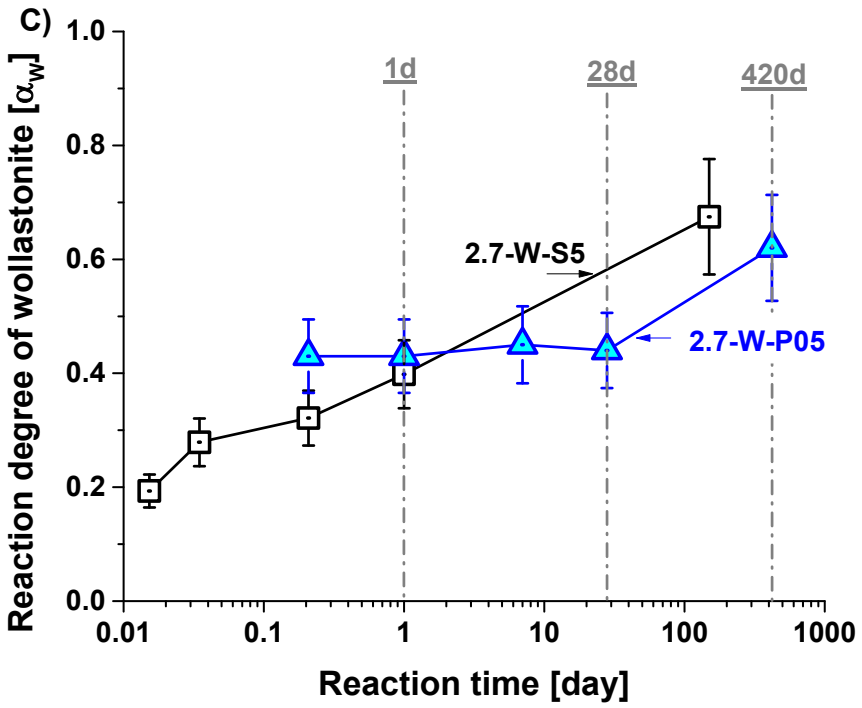


Figure 5: XRD patterns of the hydrated pastes: A) reference paste without wollastonite at w/b ratio of 0.5 (2.7-C-P05), B) paste with wollastonite at w/b ratio of 0.5 (2.7-W-P05), and C) estimated reaction degree of wollastonite corrected for bound water based on TGA results at 600 °C. P = periclase, K = $KH_2PO_4$, Q = quartz, S = K-struvite, W = wollastonite-2M, 15 = $Mg_2KH(PO_4)_2{\cdot}15H_2O$, * = unidentified phase.

The XRD results as presented above are confirmed by the TGA data shown in Figure 6. Compared to 2.7-C-P05 (see Figure 6A), 2.7-W-P05 (see Figure 6B) has K-struvite as the main phase, without the precipitation of $Mg_2KH(PO_4)_2{\cdot}15H_2O$. No weight losses are observed for 2.7-C-P05 after 600 °C, but for 2.7-W-P05 small weight losses are observed at around 700 °C. Moreover, as compared to 28 days, a weight loss increase for 2.7-W-P05 after 420 days was observed in the range of around 550 to 710 °C. The weight loss (marked by * in Figure 6B) could be attributed to calcium carbonate ($CaCO_3$), the minor impurity in wollastonite, and / or to the

possible carbonation of wollastonite [30, 51] in air over time. Also, this may be assigned to formation of $CaK_3H(PO_4)_2$ that decomposes at a similar temperature range (see Appendix A). Traces of $CaK_3H(PO_4)_2$ was found in an MKP cement paste with the same $Mg/PO_4$ molar ratio of 2.7 and a w/b ratio of 0.25 after 170 days [6]. The formation is through reaction between monticellite ($CaMgSiO_4$), the minor impurity in magnesia, and ions of $K^+$ and $HPO_4^{2-}$ in pore solution. In this study, $CaK_3H(PO_4)_2$ was also found as an intermediate product in the wollastonite – $KH_2PO_4$ suspension (W-K-S), which is destabilized to hydroxyapatite after 150 days.

The magnesia reaction degree estimated based on the results of XRD (Figure 5) and TGA (Figure 6) were 29% for 2.7-W-P05 after 28 days and 36% for 2.7-C-P05.

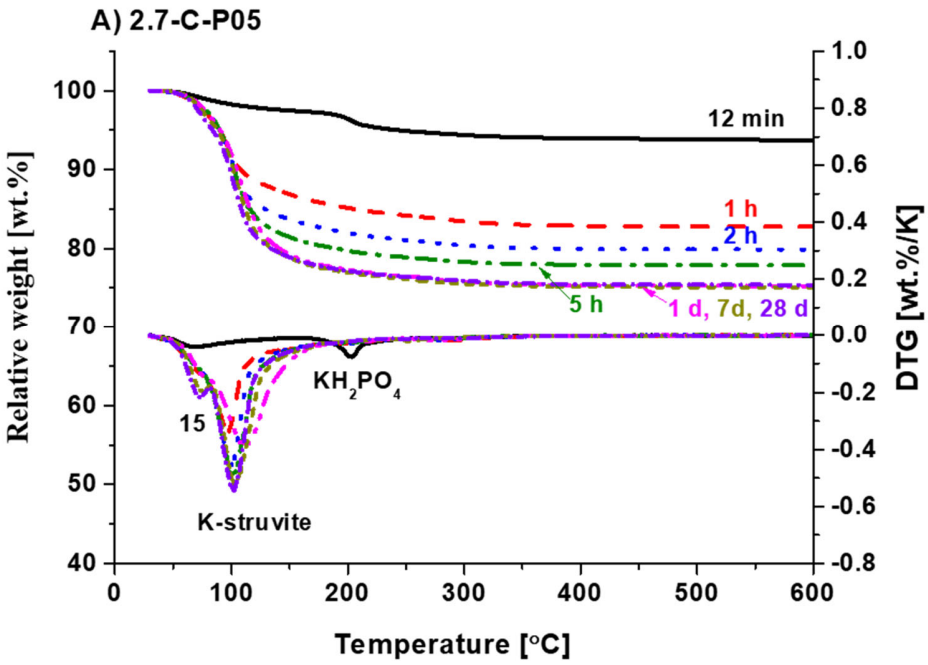

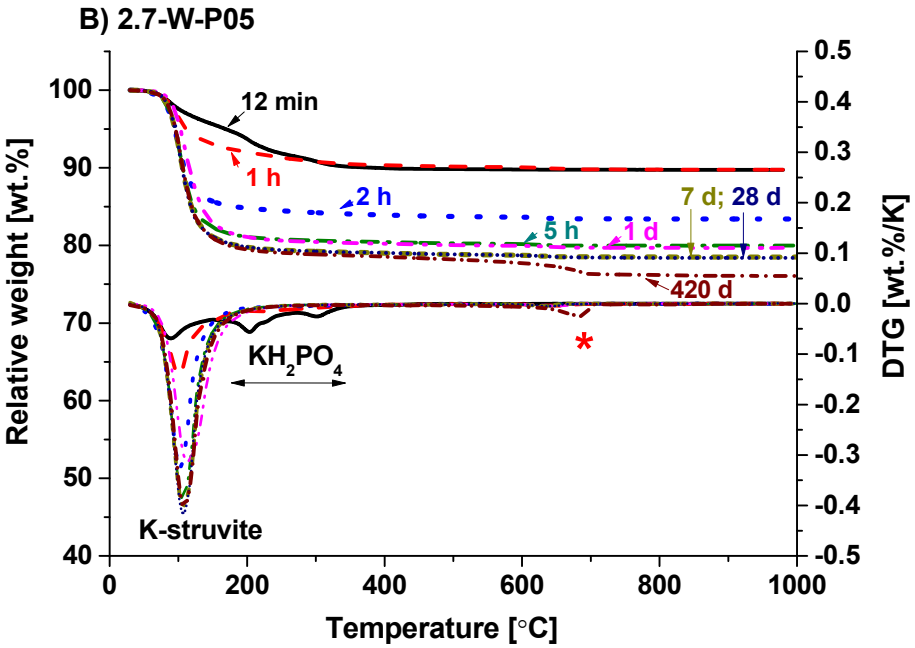


Figure 6: TGA/DTG of hydrated MKP cements with time: A) without wollastonite (2.7-C-P05) and B) with wollastonite (2.7-W-P05). 15 = $Mg_2KH(PO_4)_2{\cdot}15H_2O$, * = unidentified phase.

Figure 7A shows the $^{31}P$ NMR spectra of K-struvite, $CaK_3H(PO_4)_2$, and hydrated cements. K-struvite has a sharp resonance at around 5.6 ppm, somewhat lower than the reported values of 6.0 ppm [52], 6.2 [14], and 6.4 ppm [5]. Also a small hump centered at around 1 ppm is observed, suggesting traces of cattiite ($Mg_3(PO_4)_2{\cdot}\ 22H_2O$, 1.1 ppm [53]) in agreement with the fact that K-struvite can be partially destabilized to cattiite in the long-term [3, 7, 43]. The comparison with the resonance of K-struvite suggests the clear present of K-struvite in 2.7-C-P05 and 2.7-W-P05. Further 2.7-C-P05 shows a small shoulder centered at around 3.8 ppm corresponding possibly to $KH_2PO_4$ (3.9 ppm [5] and 3.6 [14]) and/or $Mg_2KH(PO_4)_2{\cdot}15H_2O$ (2.6 to 3.7 ppm [5]) in agreement with the XRD data in Figure 5A, and a hump centered at around 1.6 ppm corresponding to phosphorröslerrite ($MgHPO_4{\cdot}7H_2O$, 1.7 ppm [5]). In addition to $Mg_2KH(PO_4)_2{\cdot}15H_2O$,

382 phosphorröslerrite is the other phase contained in efflorescence of MKP cements [6]. In the
383 presence of wollastonite, additional humps ranging from around 4 to -3 ppm are observed for 2.7-
384 W-P05 and clearer for 2.7-W-S5, indicating presence of several relatively poorly ordered
385 phosphate environments. Resonances for brushite (1.3 ppm [54, 55]), hydroxyapatite (3.0 ppm [54,
386 55]), octacalcium phosphate (2.2 and 3.3 ppm [54, 55]) and $CaK_3H(PO_4)_2$ (0 ppm, this study) point
387 tentatively towards the possible formation of calcium phosphates. However, these broad humps are
388 also in the region where bands of magnesium phosphates are observed, making a clear assignment
389 of those bands impossible.

390 The $^{29}Si$ NMR spectrum of the unhydrated cement with wollastonite (2.7-W: unhydrated) in
391 Figure 7B shows the main resonances at around -87 and -89 ppm corresponding to the $Q^2$ site of
392 $CaSiO_3$ [56], and small ones at around -62, -66 and -110 ppm corresponding to the $Q^0$ site of
393 $Mg_2SiO_4$ [57] and $CaMgSiO_4$ [58], the minor impurities in magnesia, and to the $Q^4$ site of $SiO_2$,
394 the minor impurity in wollastonite. Compared to the unhydrated sample (2.7-W: unhydrated), the
395 hydrated cement with wollastonite (2.7-W-P05) after 420 days shows a peak broadening between
396 -80 to -100 ppm. The signals of the $Q^0$ ($Mg_2SiO_4$ and $MgCaSiO_4$) and $Q^4$ sites ($SiO_2$) disappear,
397 suggesting reaction of these minor phases. The broadening of the bands between -80 to -100 ppm
398 points towards some reaction of wollastonite and possibly to the formation of some M-S-H, which
399 has several broad bands between -80 and -100 ppm [59]. In addition the formation of some C-S-H,
400 with typical bands in the range of -78 to -86 ppm [60], cannot be excluded. These $^{31}P$ and $^{29}Si$
401 NMR investigations tentatively indicate that the reaction of wollastonite leads to the formation of
402 calcium phosphates and M-S-H, which would be consistent with the thermodynamic predictions
403 presented in Figure 4.
404

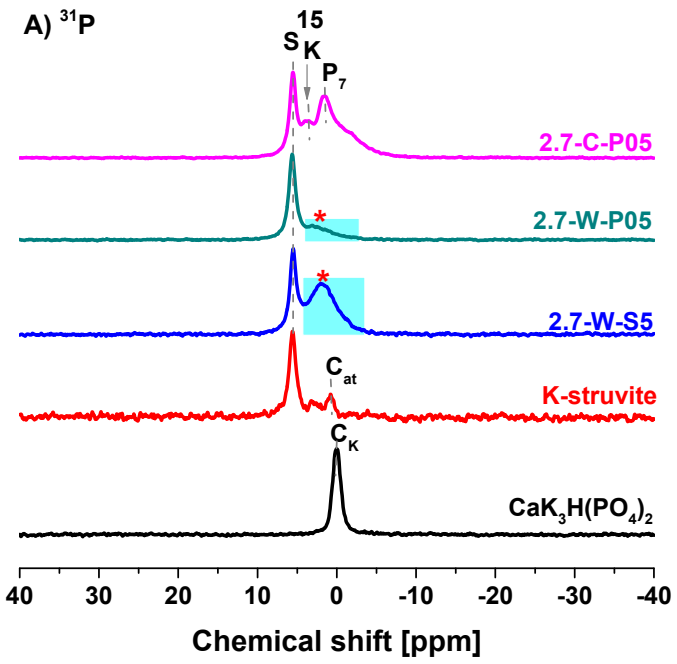


405

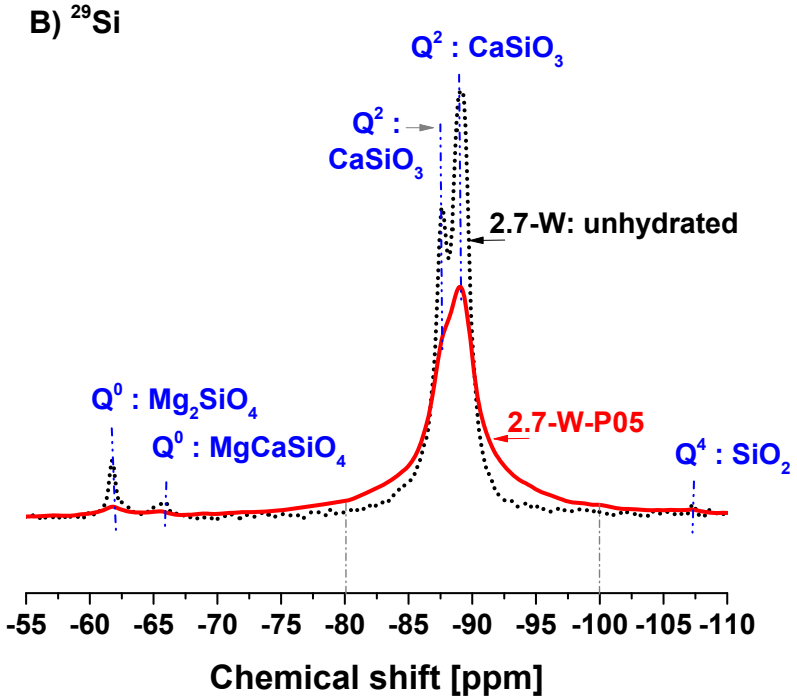


406

407 Figure 7: A) $^{31}P$ NMR spectra of K-struvite, $CaK_3H(PO_4)_2$ and hydrated cements, B) $^{29}Si$ NMR spectra of

408 unhydrated (2.7-W: unhydrated) and hydrated (2.7-W-P05) cements with wollastonite. S = K-struvite, K

409 = $KH_2PO_4$, $C_{at}$ = cattiite, $C_K$ = $CaK_3H(PO_4)_2$, $P_7$ = phosphorröslerrite, 15 = $Mg_2KH(PO_4)_2{\cdot}15H_2O$. ∗ =
410 unidentified phase. The equilibrium times for K-struvite, $CaK_3H(PO_4)_2$, 2.7-C-P05, 2.7-W-P05, and 2.7-
411 W-S05 were 740, 50, 28, 420, and 150 days, respectively. The synthesis of K-struvite is detailed in [6] and
412 that of $CaK_3H(PO_4)_2$ in Appendix A.
413
414 SEM image of the cement paste with wollastonite (2.7-W-P05) after 420 days suggested the
415 presence of mainly K-struvite with different morphologies, i.e. small platelets with well-defined
416 edges and bigger prism-like ones. Some hydrates are seen growing on wollastonite particles,
417 suggesting that wollastonite acts as nucleation site and / or as reactant. EDS analysis result on the
418 polished section of 2.7-W-P05 after 420 days are shown in Figure 8. The measured K/P and Mg/P
419 atomic ratios fall in the range of 0.5 – 1.0 and 0.6 – 1.3, of which the corresponding average values
420 are calculated as 0.8 ± 0.12 and 0.9 ± 0.20. This indicates a possible mix of K-struvite with
421 $Mg_2KH(PO_4)_2{\cdot}15H_2O$ although no clear evidences of the presence of $Mg_2KH(PO_4)_2{\cdot}15H_2O$ was
422 obtained by XRD, TGA and $^{31}P$ NMR analyses, or alternatively the presence of K-struvite with
423 more P (or less K) in its structure. Most the measured Si/Ca atomic ratios are around 1
424 corresponding to the presence of wollastonite in the interaction volume of the electron beam. Most
425 measured P/Ca atomic ratios are less than 2.0, the stoichiometric value of $CaK_3H(PO_4)_2$, indicating
426 a possible mix of wollastonite and calcium phosphate hydrates, such as hydroxyapatite,
427 octacalcium phosphate, brushite and $CaK_3H(PO_4)_2$.

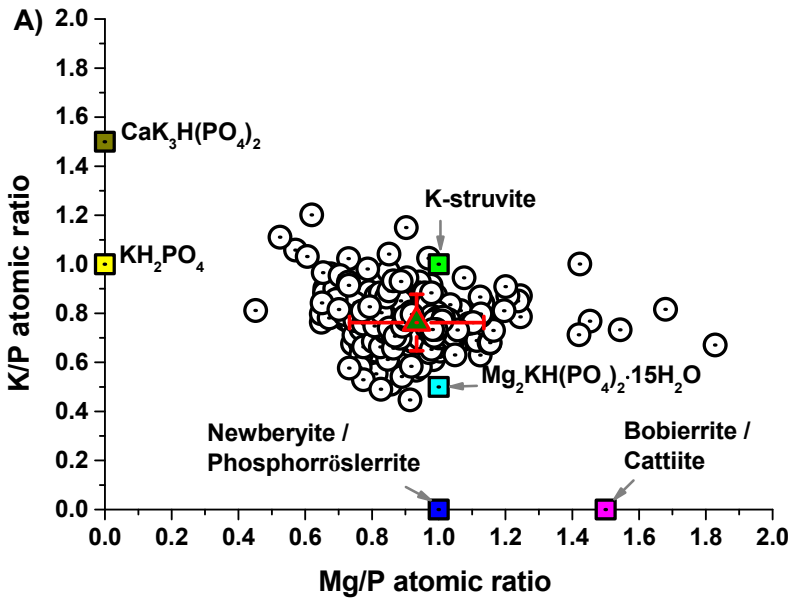


428

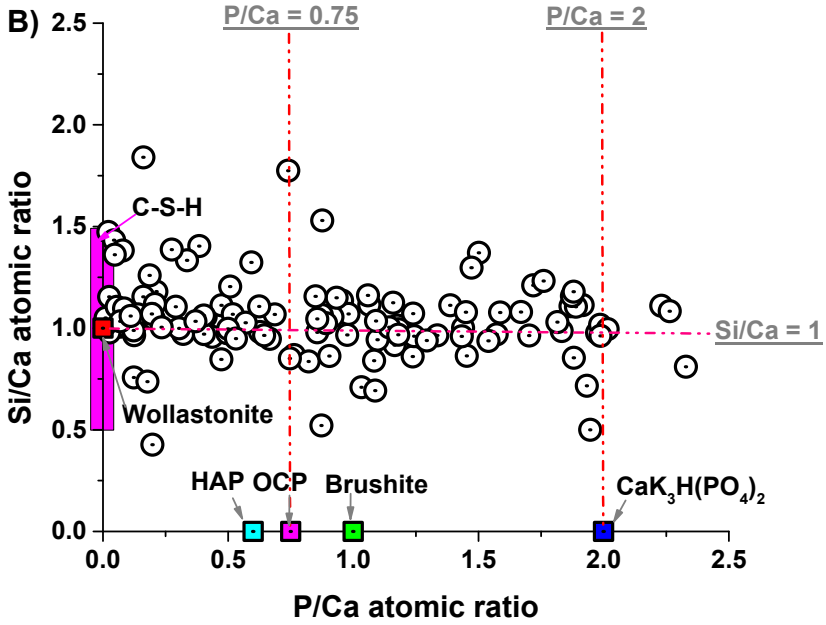


429

430 Figure 8: Results of EDS analysis on a polished section of the hydrated cement paste (2.7-W-P05) after

431 420 days of hydration. HAP = hydroxyapatite; OCP = octacalcium phosphate.

432

433

### 3.1.5 Pore solution chemistry

Compositions of the pore solution of the hydrated cement pastes (2.7-C-P05 and 2.7-W-P05) are summarized in Table 4, and shown in Figure 9A. Large changes in the pore solution compositions are observed, especially during the first day. In the absence of wollastonite, the total concentrations of K and phosphate of 2.7-C-P05 after 5 hours are strongly reduced and the Mg concentration drops below the detection limit of 0.04 mM. The formation of K-struvite from magnesia and $KH_2PO_4$ during the first 5 hours (see Figure 5A and Figure 6A) leads to a fast pH increase to around 12. The concentrations of K and phosphate decrease at slower rates after 5 hours and reach stable values after 1 day and longer as well as the pH values. This suggests that the hydration kinetics is slowed down after 5 hours in agreement with the calorimetric results in Figure 3. Even in the absence of wollastonite, low concentrations of Ca and Si are measured due to the presence of minor $Mg_2SiO_4$ and $CaMgSiO_4$ in the magnesia used. Compared to the limited change of the Ca concentrations, the Si concentrations strongly decrease during the first 5 hours.

The trends of the pore solution compositions of the sample with wollastonite (2.7-W-P05) are similar to those of 2.7-C-P05; however, the total concentrations of K, Mg and phosphate of 2.7-W-P05 after 10 min are around half the values of 2.7-C-P05 due to the dilution of cement by wollastonite. The K, Mg and phosphate concentrations decrease slower in the presence of wollastonite so that the K and phosphate concentrations after 28 days are around 7 times higher compared to 2.7-C-P05. The initial Ca and Si concentrations are similar as for 2.7-C-P05; however, the Si concentration increases with time, which is consistent with the observed reaction of wollastonite. The presence of wollastonite leads to lower pH values, i.e. around 10.8 after 28 days, which is attributed to the dilution effect of wollastonite and the changed hydration path.

Effective saturation indices with respect to possible hydrates are calculated using the analytical data of the pore solutions given in Table 4 and the thermodynamic data in Table 3. Figure 9B and

C show the data for the selected hydrates such as K-struvite, phosphorrösslerite, newberyite, $Mg_2KH(PO_4)_2 \cdot 15H_2O$, brushite, hydroxyapatite, octacalcium phosphate, $CaK_3H(PO_4)_2$, M-S-H and C-S-H. For 2.7-C-P05, phosphorröslerrite, newberyite, and $Mg_2KH(PO_4)_2 \cdot 15H_2O$ are oversaturated after 10 min, and become undersaturated afterwards. Hydroxyapatite and octacalcium phosphate, in contrast, are undersaturated initially and oversaturated afterwards. K-struvite and M-S-H are potentially slightly oversaturated after 10 min and longer. And brushite, $CaK_3H(PO_4)_2$, and C-S-H are always undersaturated, informing their formation is not probable. Note that the precipitation is expected to be slower than that of brushite or octacalcium phosphate [61]; and not every oversaturated hydrate necessarily precipitated as the formation might be kinetically hinder [38].

Similar to 2.7-C-P05, K-struvite in 2.7-W-P05 is always oversaturated with time, but the oversaturation degree is slightly higher. Phosphorröslerrite is oversaturated only after 10 min, while newberyite and $Mg_2KH(PO_4)_2 \cdot 15H_2O$ are still oversaturated after 5 hours, which agrees with the lower pore solution pH as given in Table 4. Brushite is oversaturated only after 5 hours, indicating its possible presence as an intermediate hydrate; while hydroxyapatite, octacalcium phosphate and M-S-H are oversaturated after 5 hours and longer. Compared to 2.7-C-P05, the oversaturation degree of M-S-H is slightly higher, indicating a more likely precipitation in 2.7-W-P05. The undersaturation of $CaK_3H(PO_4)_2$ and C-S-H with time also suggest their formation is not probable.

482 Table 4: Measured total concentrations and pH values in the pore solution of the hydrated cements

| Time | Na [mM] | K [mM] | Mg [mM] | Ca [mM] | Si [mM] | $PO_4$ [mM] | Cl [mM] | pH[a] |
|---|---|---|---|---|---|---|---|---|
| ***2.7-C-P05 (MKP cement paste)*** | | | | | | | | |
| **10 [min]** | 34 | 7450 | 1691 | <0.001 | 36 | 7639 | n.a. | 6.0 |
| **5 [h]** | 7.5 | 807 | <0.04 | 1.8 | 2.2 | 307 | n.a. | 12.1 |
| **1 [d]** | 15 | 135 | <0.04 | 0.81 | 2.7 | 46 | n.a. | 12.1 |
| **7 [d]** | 38 | 126 | <0.04 | 0.84 | 0.09 | 27 | n.a. | 12.4 |
| **28 [d]** | 55 | 125 | <0.04 | 0.78 | 0.05 | 41 | n.a. | 12.4 |
| ***2.7-W-P05 (MKP cement paste with wollastonite)*** | | | | | | | | |
| **10 [min]** | 19 | 3173 | 875 | <0.001 | 21 | 3699 | 0.59 | 5.9 |
| **5 [h]** | 24 | 2202 | 12 | 0.72 | 12 | 1295 | 0.82 | 8.1 |
| **1 [d]** | 36 | 1214 | <0.04 | 0.62 | 36 | 540 | 0.96 | 10.8 |
| **7 [d]** | 21 | 975 | <0.04 | 0.49 | 28 | 399 | 1.1 | 10.6 |
| **28 [d]** | 20 | 837 | <0.04 | 0.39 | 45 | 280 | 1.2 | 10.8 |
| ***2.7-C-S5 (MKP cement suspension)*** | | | | | | | | |
| **22 [min], P1** | 4.5 | 798 | 56 | 3.6 | 4.7 | 748 | n.a. | 6.5 |
| **50 [min]** | 6.0 | 269 | 6.0 | 0.80 | 5.1 | 175 | n.a. | 7.6 |
| **66 [min], P2** | 5.9 | 138 | 3.9 | 0.52 | 4.9 | 93 | n.a. | 7.8 |
| **185 [min]** | 5.9 | 97 | <0.04 | 0.26 | 4.5 | 51 | n.a. | 11.1 |
| **7 [d]** | n.a. | 48 | <0.04 | 0.01 | 3.3 | 5.7 | n.a. | 11.7 |
| ***2.7-W-S5 (MKP cement suspension with wollastonite)*** | | | | | | | | |
| **22 [min], P1** | 3.0 | 458 | 31 | 2.5 | 4.1 | 419 | n.a. | 6.9 |
| **50 [min]** | 2.9 | 400 | 11 | 1.3 | 5.2 | 119 | n.a. | 7.7 |
| **89 [min], P2** | 3.6 | 156 | 3.3 | 0.64 | 3.6 | 114 | n.a. | 7.9 |
| **140 [min]** | 3.5 | 282 | 4.8 | 0.35 | 4.2 | 191 | n.a. | 7.8 |
| **5 [h]** | 3.5 | 233 | 4.2 | 0.32 | 3.8 | 154 | n.a. | 7.8 |
| **120 [d]** | <0.001 | 183 | <0.04 | 0.01 | 8.2 | 91 | n.a. | 10.2 |
| ***Detection limit*** | | | | | | | | |
| | 0.001 | 0.001 | 0.04 | 0.001 | 0.002 | 0.001 | 0.001 | |

483 [a]: pH was measured at 23 °C. n.a.: not analyzed.

484

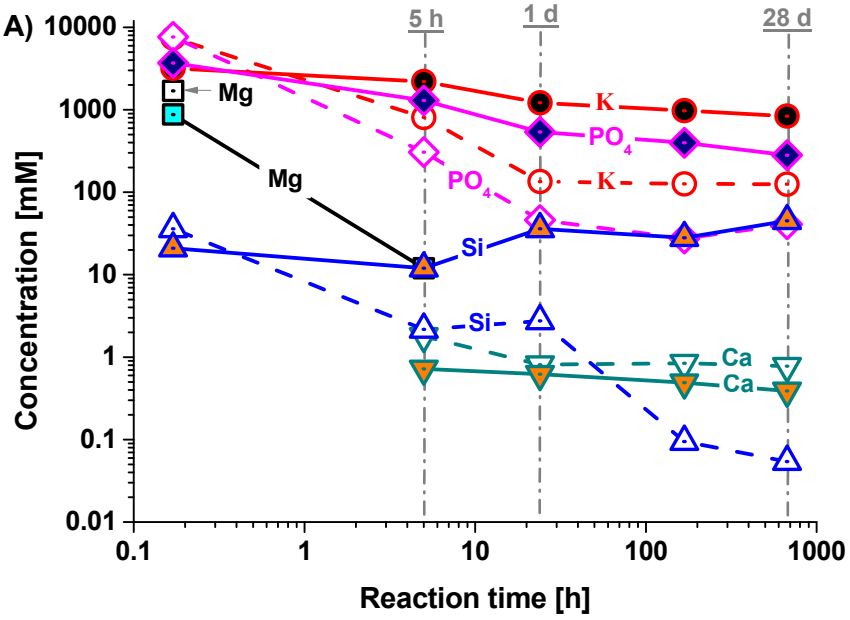
A) 10000
5 h
1 d
28 d
Mg
Mg
K
PO4
PO4
K
Si
Si
Ca
Ca
Concentration [mM]
0.01
0.1
1
10
100
1000
0.1
1
10
100
1000
Reaction time [h]

485

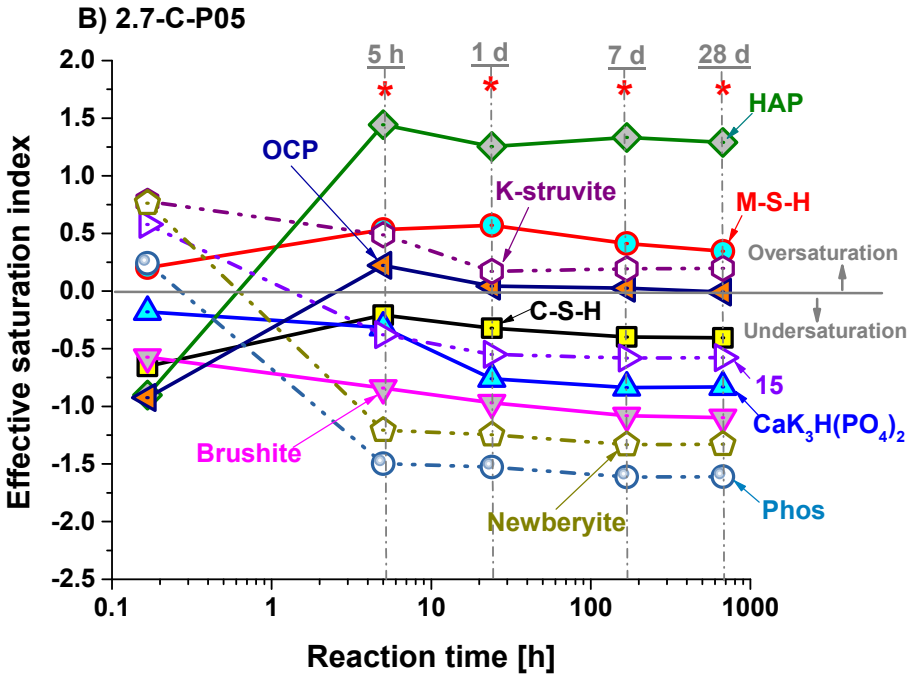
B) 2.7-C-P05
5 h
1 d
7 d
28 d
HAP
OCP
K-struvite
M-S-H
Oversaturation
C-S-H
Undersaturation
15
CaK3H(PO4)2
Brushite
Newberyite
Phos
Effective saturation index
2.0
1.5
1.0
0.5
0.0
-0.5
-1.0
-1.5
-2.0
-2.5
0.1
1
10
100
1000
Reaction time [h]

486

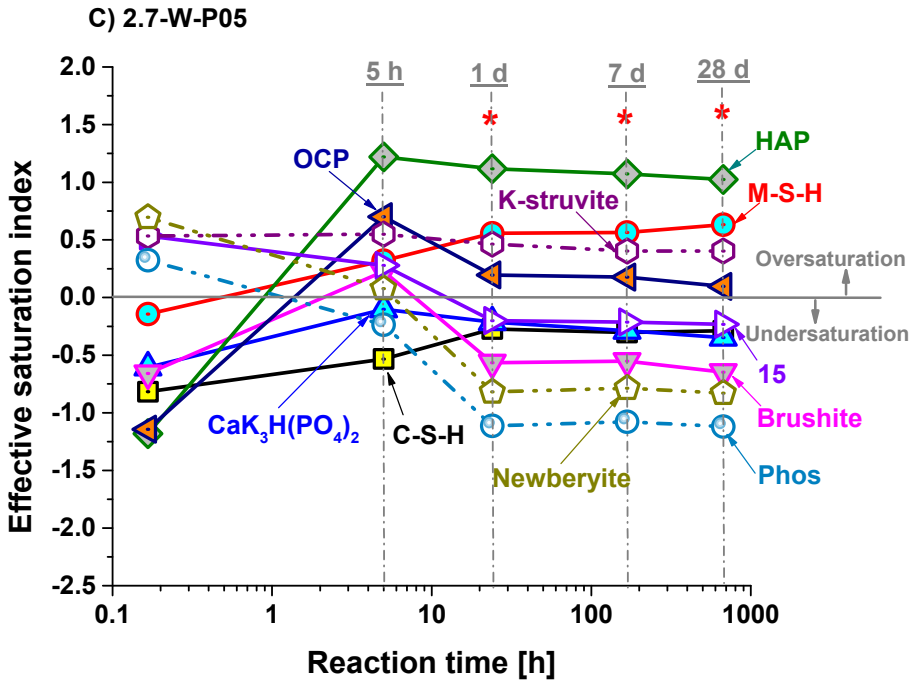


Figure 9: A) Total ion concentrations of the pore solutions of the hydrated pastes (2.7-C-P05 and 2.7-W-P05). Data for 2.7-C-P05 are represented by the empty symbols and connected by dashed lines, and data for 2.7-W-P05 are by filled symbols and connected by solid lines. B) and C) calculated effective saturation indices. *: upper limit of SI: the detection limit of Mg (0.04 mM) were used for the samples where the Mg concentrations were below the detection limit. C-S-H = calcium silicate hydrate, HAP = calcium hydroxyapatite, M-S-H = magnesium silicate hydrate, OCP = octacalcium phosphate, Phos = phosphorrösslerite, 15 = $Mg_2KH(PO_4)_2 \cdot 15H_2O$.

## 3.2 Suspensions

The investigations on the pastes as presented above indicate a reaction of wollastonite in MKP cement, and point towards the formation of some calcium phosphate hydrates and M-S-H. However, the experimental evidences are not too clear. Thus, in a second series of experiments, the cements were investigated at a much higher w/b ratio of 5, under which a more complete hydration could

501 be expected although the hydration path could be changed as compared to those at low w/b ratios.
502 In addition, the reaction of wollastonite with $KH_2PO_4$ only and of wollastonite with magnesium
503 was investigated separately to determine composition of the hydrates from the dissolution of
504 wollastonite.
505
506 3.2.1 Wollastonite - $KH_2PO_4$ suspension
507 The wollastonite - $KH_2PO_4$ suspension reacted fast initially, leading to a rapid pH increase to
508 around 9 and a reaction degree of wollastonite of around 67 % after 7 days. Afterwards, the reaction
509 slowed down, leading to a pH value of around 10.4 and a wollastonite reaction degree of around
510 80 % after 340 days. The XRD results (see Appendix B-a) of the suspension with time suggests
511 the formation of brushite ($CaHPO_4 \cdot 2H_2O$) and $CaK_3H(PO_4)_2$ during the first few hours and days
512 and their later-on destabilization to a poorly crystalline hydroxyapatite ($Ca_5(PO_4)_3(OH)$) after 7
513 days and longer.
514
515 3.2.2 Wollastonite - $MgCl_2$ / MgO suspensions
516 Reaction of wollastonite blended with magnesium (magnesia or $MgCl_2$) was also investigated.
517 In the presence of magnesia, the pH value of the suspension (W-MgO-S) after 110 days was around
518 11; further non or very little wollastonite was reacted and the hydrolysis of magnesia leads to
519 formation of brucite. However, the presence of $MgCl_2$ leads to a much lower pH value of around
520 7.2 after 180 days and an almost complete reaction of wollastonite, of which the reaction degree is
521 estimated as 97 %. M-S-H is formed in W-MgCl-S, which is identified by two typical broad humps
522 centered at 22.9 and 41.0 ° 2θ CoKα (d-spacing values: 4.5 and 2.6 Å) [59, 62, 63] in XRD analysis
523 (see Appendix B-b). This also confirmed by the EDS analysis presented in Figure 10. An average

Mg/Si atomic ratio of around 1 is observed for the M-S-H as well as the uptake of some Ca as suggested by average Ca/Si atomic ratio of 0.10 ± 0.03, in good agreement with the findings of [44, 64, 65] .

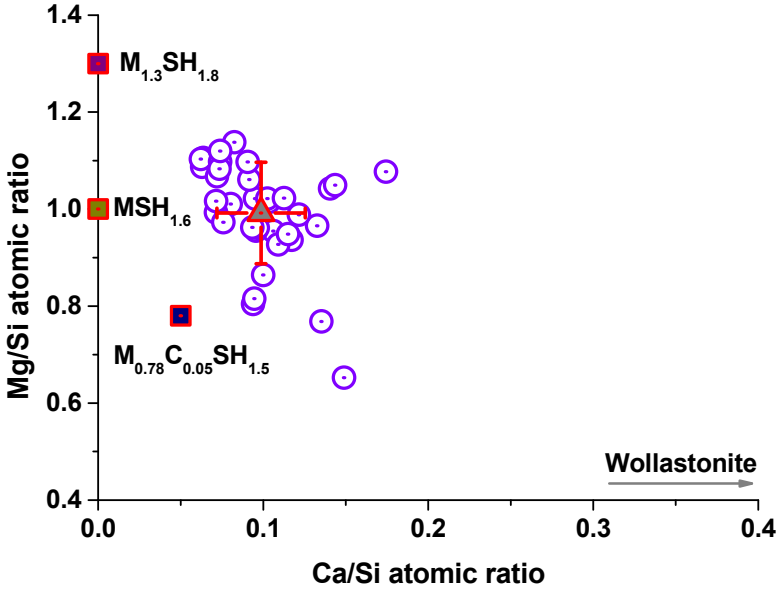


Figure 10: EDS analysis on solids of W-MgCl-S after 180 days equilibration at 50 °C.

The data shown in this section confirm the reaction of wollastonite with $KH_2PO_4$ or magnesium, especially under low pH conditions, suggesting hydroxyapatite and M(-C)-S-H as potential hydrates for MKP cements containing wollastonite.

### 3.2.3 Cement suspensions

#### 3.2.3.1 Reaction kinetic

Changes of the electrical conductivity and pH of the cement suspensions (2.7-C-S5 and 2.7-W-S5) with time are shown in Figure 11. Results of both the conductivity and pH of the cement

539 suspensions suggest fast reactions that are almost finished after the first 8 hours. Compared to the
540 reference cement suspension (2.7-C-S5), the presence of wollastonite in 2.7-W-S5 leads to the
541 second peak (P2) occurring later and to a less distinct decrease of conductivity, indicating a slowed
542 down reaction kinetics and possibly a changed reaction path. Note that the lower initial
543 conductivity of 2.7-W-S5 as compared to 2.7-C-S5 is due to the presence of less $KH_2PO_4$ in the
544 binder.
545

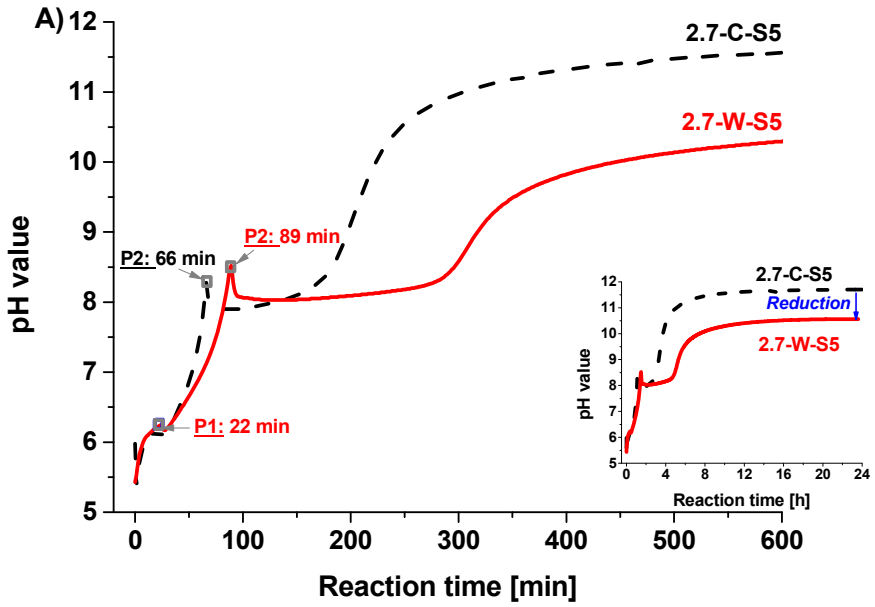


546

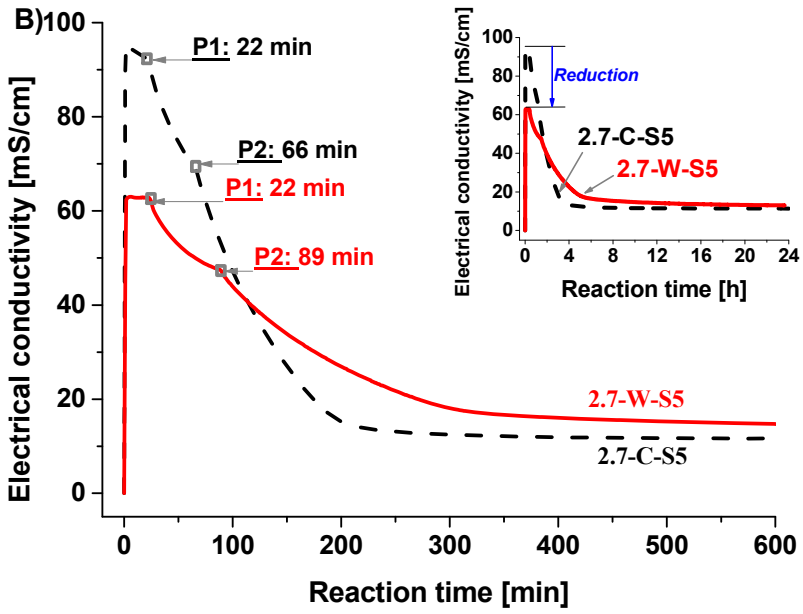


Figure 11: Development of A) pH, and B) electrical conductivity in cement suspensions (2.7-C-S5 and 2.7-W-S5) with time. P1 = 1st peak, P2 = 2nd peak. Data of 2.7-C-S5 were taken from [6].

3.2.3.2 Hydrates

As for the reference cement paste (2.7-C-S5) [6], 2.7-W-S5 (see Appendix C) both newberyite and K-struvite formed at early times, and newberyite is destabilized to K-struvite with time. $Mg_2KH(PO_4)_2{\cdot}15H_2O$ also appears as an intermediate phase and is destabilized to K-struvite after 5 hours. Further the comparison of the XRD patterns of wollastonite and hydrated cement suspensions confirms K-struvite as the only crystalline hydrate in 2.7-W-S5 in the long-term, suggesting that the observed broad hump ranging at around 4 to -3 ppm in the $^{31}P$ NMR spectrum in Figure 7A is most likely due to the presence of calcium phosphate hydrates rather than associated with magnesium phosphate hydrates. As shown in Figure 12, the reflection of K-struvite in 2.7-W-S5 compared to 2.7-C-S5 are slightly shifted and several small reflections at 2θ CoKα 34.6, 35.6,

and 36.2 ° (d-space values: 3.0, 2.9 and 2.9 Å) disappear, which could be due to the presence of wollastonite and the formation of additional hydrates. Again, no crystalline hydroxyapatite was observed to be formed, indicating rather the formation of an amorphous calcium phosphate. It has been observed that the Mg can partially be incorporated in hydroxyapatite, which leads to lower degree of ordering in hydroxyapatite and broad XRD signals [66, 67].

The estimated reaction degree of wollastonite in 2.7-W-S5 (see Figure 5C) shows a fast reaction during the first 1.5 hours when the pH of the suspension is below 8, and a slowed down reaction afterwards. The higher reaction degree of wollastonite in 2.7-W-S5 than of 2.7-C-P05 over long-term could be attributed to the higher availability of water and the lower pH condition as presented in Table 4.

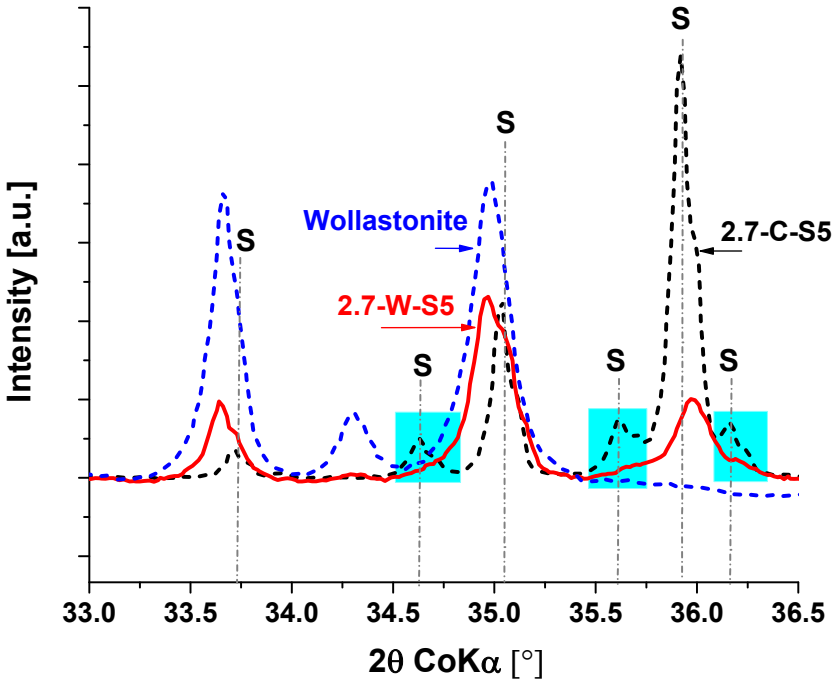


Figure 12: XRD patterns of wollastonite and hydrated cements without (2.7-C-S5 after 7 days) and with (2.7-W-S5 after 150 days) wollastonite. S = K-struvite

575 Figure 13 schematically summarizes the solid phase changes in the cement suspensions;
576 however, for the hydrates, only magnesium phosphate hydrates are considered. The comparison
577 shows that the presence of wollastonite suppresses phosphorrösslerite formation, delays
578 $Mg_2KH(PO_4)_2 \cdot 15H_2O$ and its destabilization to K-struvite, and slows down the pH increase.

579

580

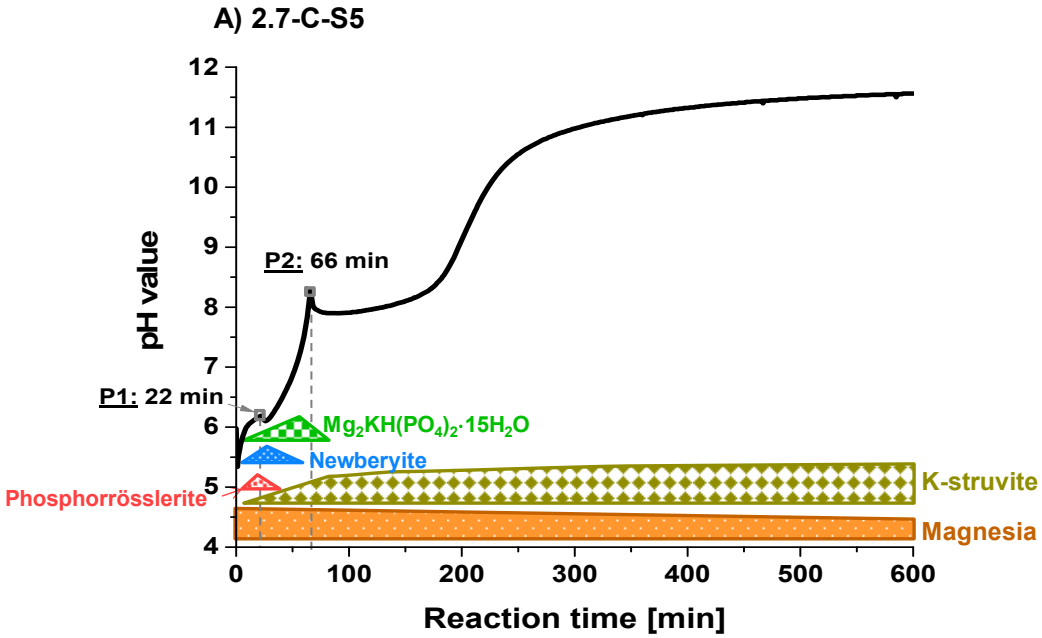


581

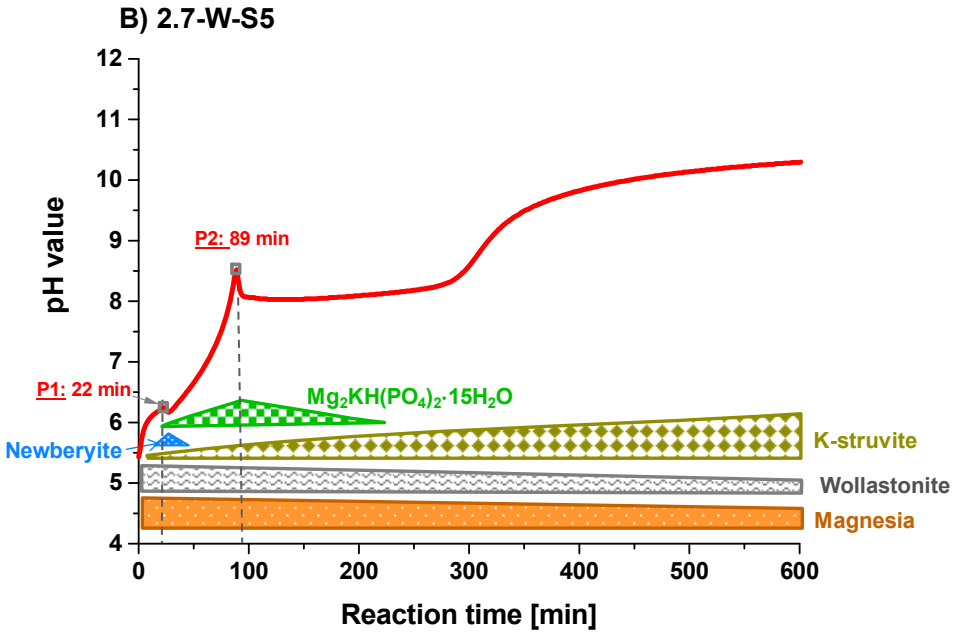


582

583 Figure 13: Schematic cement hydration paths. A) reference cement suspension without wollastonite (2.7-
584 C-S5) [6], B) cement suspension with wollastonite (2.7-W-S5). Additional hydrates formed from the
585 dissolution of wollastonite in the cement suspension are not included. The hydrates presented were from
586 the results of XRD and TGA analyses.

587

588 Figure 14 shows the BSE image and EDS analysis on a polished section of the solids of 2.7-W-
589 S5 after 150 days. In addition to K-struvite, hydrates with loosely packed texture, e.g. the marked
590 area 1# in Figure 14A are observed surrounding wollastonite particles and the dark grey phase, e.g.
591 the marked area 2#. Results of the EDS analyses show that the measured average K/P and Mg/P
592 atomic ratios of K-struvite are 0.8 ± 0.2 and 1.0 ± 0.3, close to the measurement results for 2.7-W-
593 P05 (see Figure 8A). However, the phases as in the marked areas 1# and 2# have much lower
594 average K/P and Mg/P atomic ratios of 0.4 ± 0.2 and 0.4 ± 0.2. Moreover, those phases have almost
595 all of the measured P/Ca atomic ratios less than 0.75 and the average value of 0.5 ± 0.16, very close

596 to stoichiometric value of hydroxyapatite. Thus, this suggests a most likely mix of wollastonite, K-

597 struvite and hydroxyapatite in the interaction volume of the electron beam.

598

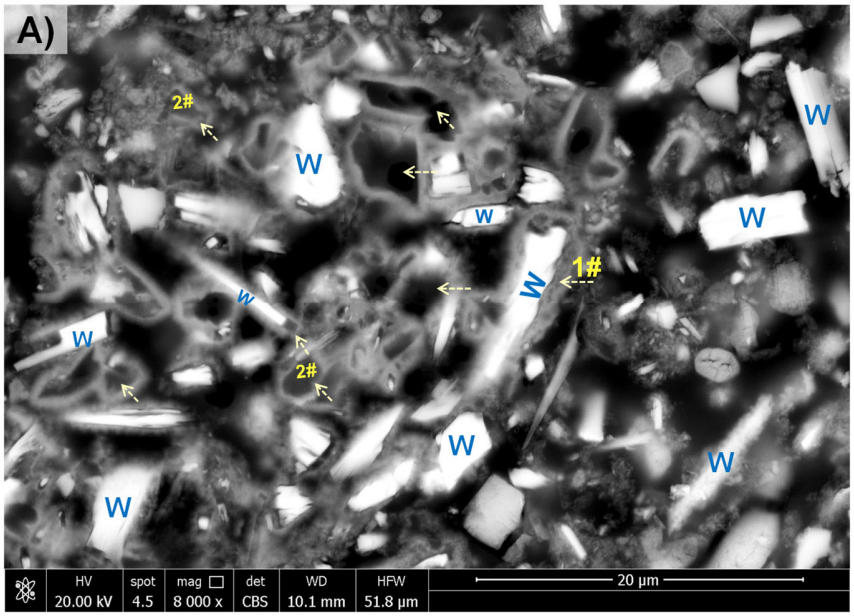


599

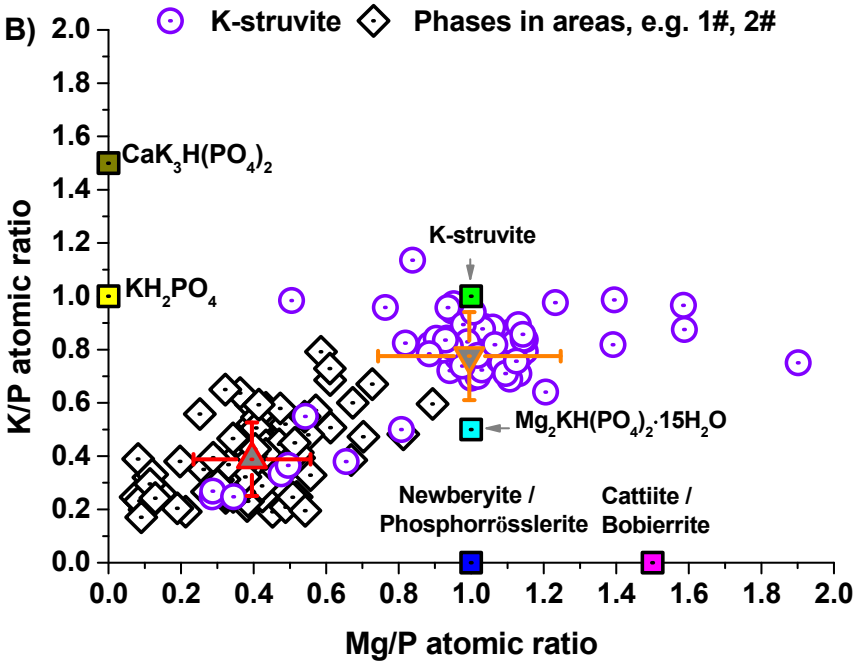


600

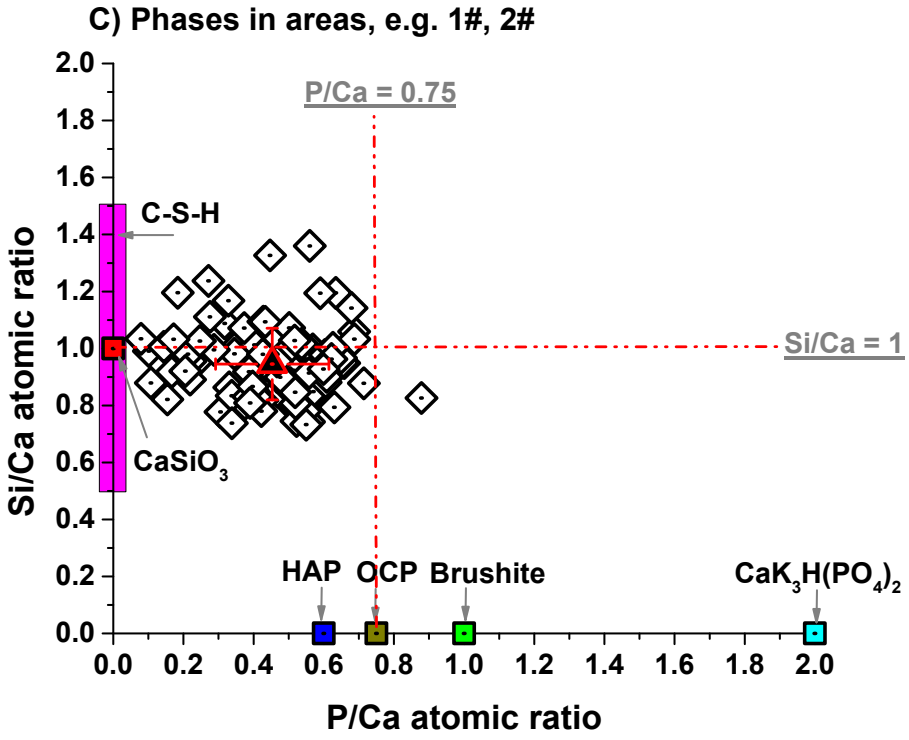


601

602 Figure 14: A) BSE image, B) and C) results of EDS analyses on a polished section of the solids of cement
603 suspension with wollastonite (2.7-W-S5) after 150 days. W= wollastonite, HAP = hydroxyapatite, OCP =
604 octacalcium phosphate.

605

606 3.2.3.4 Aqueous phase composition

607 The aqueous phase compositions of the hydrated cement suspensions with time are shown in
608 Figure 15, and are summarized in Table 4 as well. Similar to the paste system, the initial total K,
609 Mg and phosphate concentration of 2.7-W-S5 are lower compared to the reference cement
610 suspension (2.7-C-S5) due to the dilution effect of wollastonite. Further the total K, Mg and
611 phosphate concentration of 2.7-W-S5 decrease in much slower rates, as a result, the total Mg
612 concentration after 5 hours is still 4.2 mM and the total K and phosphate concentrations after 120
613 days are 183 and 91 mM. The total Ca concentrations of both suspensions decrease with time

614 although their amounts are quite small. Also, the total Si concentration of the suspensions are small.
615 Different from the minor changes in 2.7-C-S5, the total Si concentration in 2.7-W-S5 tends to
616 increase after 5 hours and later, similar to the finding in 2.7-W-P05. Figure 15B and C compares
617 the changes of $K^+$ and $Mg^{2+}$ activities in the suspensions determined by ion selective electrodes
618 with the total concentration measured by IC. Generally, the $K^+$ activities over time agree with the
619 total K concentration by IC, especially for 2.7-W-S5. The $K^+$ activities in the suspensions are close
620 up to 89 min; afterwards, 2.7-W-S5 demonstrates higher $K^+$ activities over time, in agreement with
621 the IC results. Comparable $Mg^{2+}$ activities are observed for the suspensions as well at the earlier
622 stage before 50 min; afterwards, 2.7-W-S5 shows higher $Mg^{2+}$ activities.
623

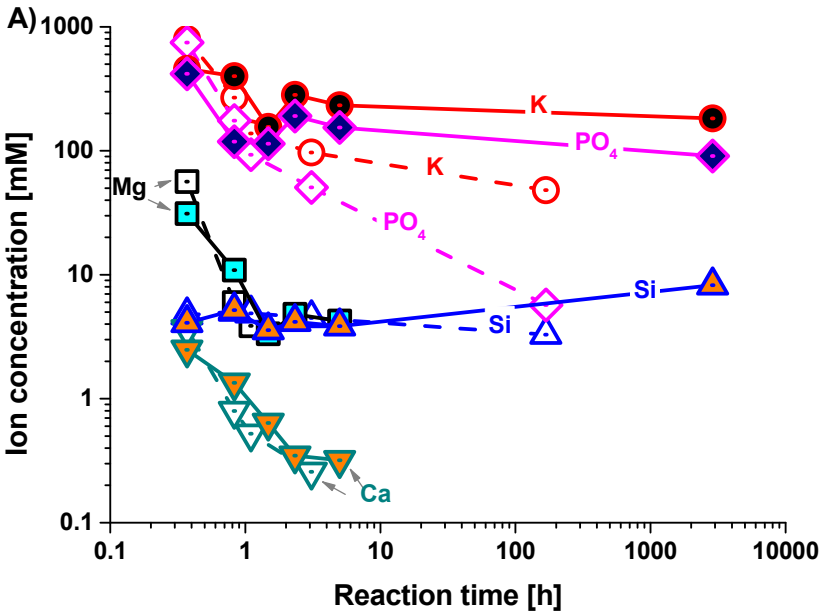


624

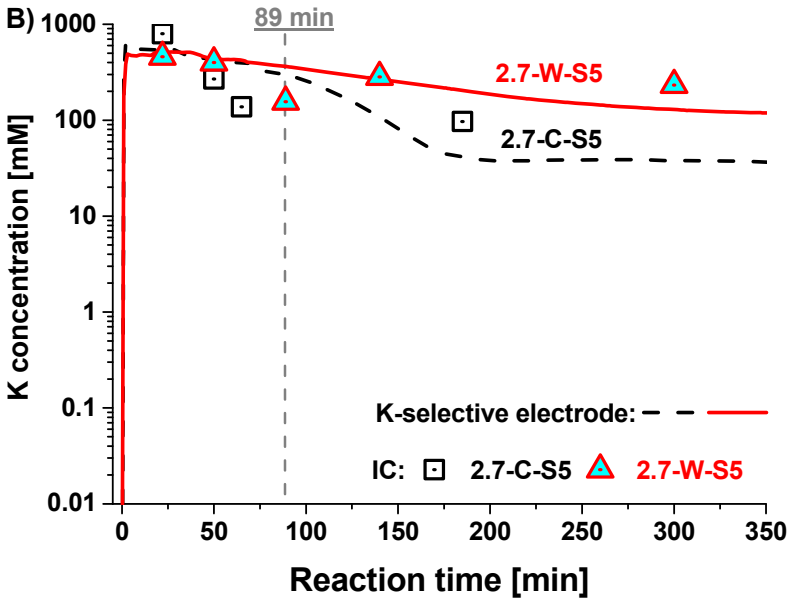


625

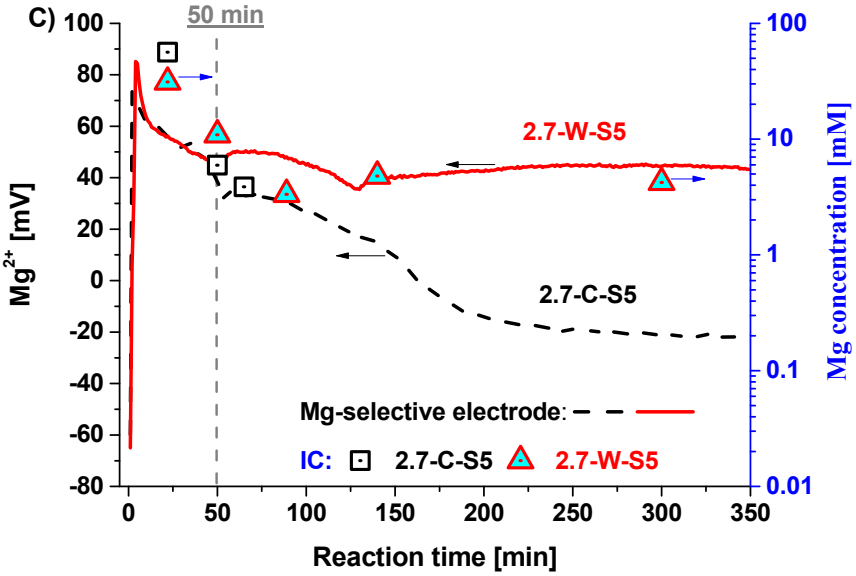


626

627 Figure 15: Hydrated cement suspensions without (2.7-C-S5) / with (2.7-W-S5) wollastonite with time. A)
628 total concentrations of Si, Ca, Mg, K and phosphate measured by IC, B) $K^+$ and C) $Mg^{2+}$ activities
629 measured by selective electrodes and compared with the total concentrations by IC. The data of 2.7-C-S5
630 were taken from [6]. The empty symbols connected by dashed lines represent 2.7-C-S5, and the filled

symbols connected by solid lines are for 2.7-W-S5. The initial total concentrations of K and phosphate of 2.7-C-S5 are 817 mM; and their initial total concentrations of 2.7-W-S5 are 490 mM.

Figure 16 shows the calculated effective saturation indices of the selected hydrates using the analytical data of the solutions given in Table 4 and the thermodynamic data in Table 3. At high w/b ratio, K-struvite and hydroxyapatite are oversaturated with time in the suspensions; further the oversaturation degree of hydroxyapatite tends to decrease with time. In contrast, C-S-H and $CaK_3H(PO_4)_2$ are undersaturated with time, indicating their absence. Phosphorrösslerite, newberyite, $Mg_2KH(PO_4)_2{\cdot}15H_2O$, brushite and octacalcium phosphate in the suspensions are oversaturated at early stage and become undersaturated later due to the destabilization at high pH conditions [4-6, 16, 61]. Compared to 2.7-C-P5, their precipitations in 2.7-W-S5 would persist longer due to the lower pH condition. M-S-H is undersaturated at early stage and becomes oversaturated later; moreover, the precipitation of M-S-H in 2.7-W-S5 would takes much longer time as compared to 2.7-C-S5.

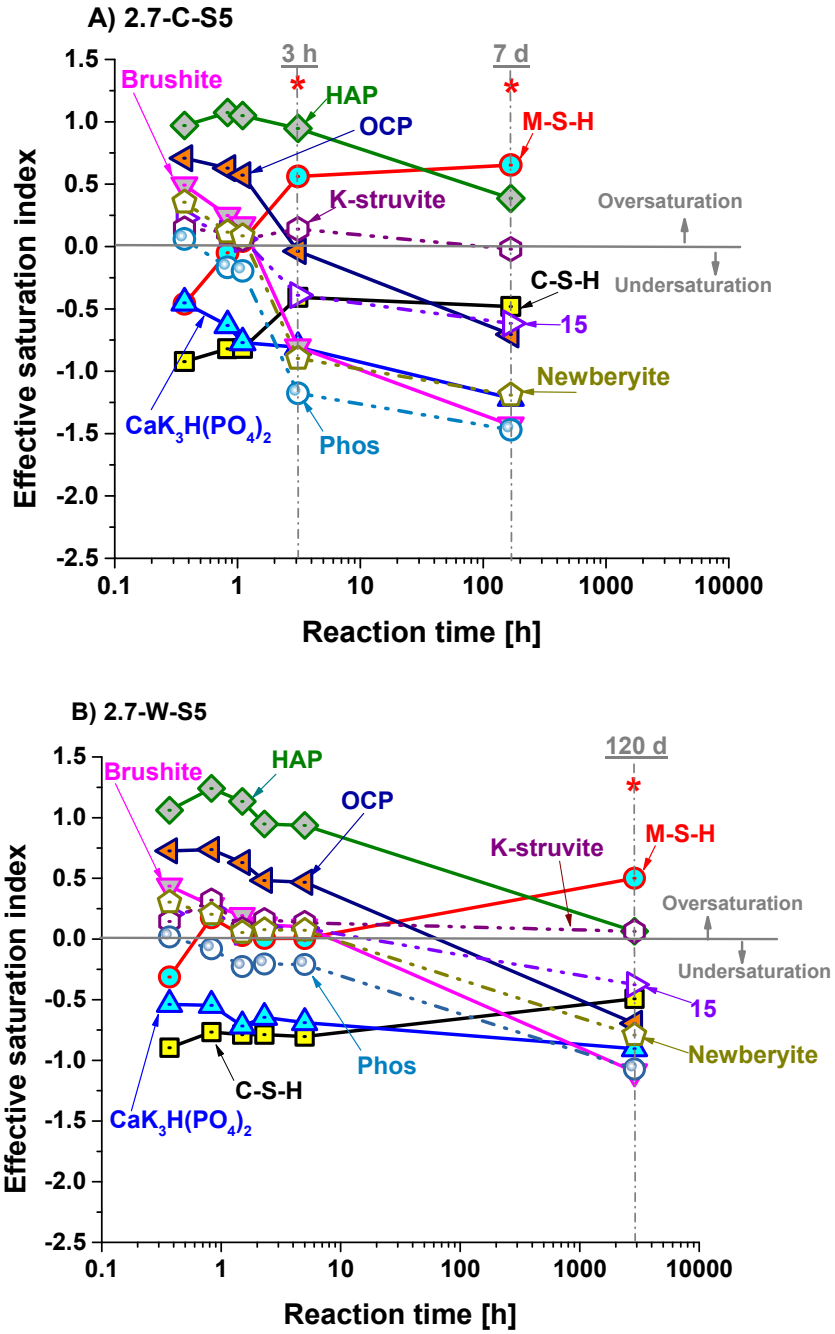


Figure 16: Calculated effective saturation indices with respect to possible hydrate precipitations in: A) cement suspension without wollastonite (2.7-C-S5), and B) cement suspension with wollastonite (2.7-W-S5). *: upper limit of SI: the detection limit of Mg (0.04 mM) were used for the samples where the Mg concentrations were below the detection limit. C-S-H = calcium silicate hydrate, HAP = calcium

652 hydroxyapatite, M-S-H = magnesium silicate hydrate, OCP = octacalcium phosphate, Phos =
653 phosphorrösslerite, 15 = $Mg_2KH(PO_4)_2 \cdot 15H_2O$.

654
655 The detailed studies in diluted suspensions indicated a higher reaction degree of wollastonite
656 and the formation of the same hydrates as in the paste samples, i.e. the formation of K-struvite and
657 probably M-S-H and amorphous hydroxyapatite.

658

659 **4 Conclusions**

660 This study investigated the effect of wollastonite on the hydration and properties of MKP
661 cements. Based on the presented findings, the following conclusions can be drawn.

662 The presence of wollastonite can prevent cement segregation at high w/b ratio and suppress
663 efflorescence. Wollastonite also increased compressive and flexural strength, in particular after 28
664 days and longer, due to the reaction of wollastonite with the magnesium and phosphate.

665 Thermodynamic calculations indicated that the reaction of wollastonite in an MKP cement is
666 expected to lead to the partial destabilization of K-struvite and to the formation of M(-C)-S-H and
667 hydroxyapatite. Experimental evidences of cement hydrate assemblages from $^{31}P$, $^{29}Si$ NMR and
668 SEM/EDS analyses confirm the reaction of wollastonite in cement and suggest hydroxyapatite
669 (amorphous) and M-S-H to be the main hydrates in addition to K-struvite. Also the calculation of
670 saturation indices based on the measured composition of the aqueous phase point towards the
671 precipitation of hydroxyapatite and M-S-H in MKP cement with wollastonite present.

672 The formation of hydroxyapatite and M-S-H was also observed in additional experiments,
673 where wollastonite reacted with only $KH_2PO_4$ or with only $MgCl_2$. With only $KH_2PO_4$ wollastonite
674 reacted to hydroxyapatite and Mg $Cl_2$ to M-(-C)-S-H.

675

## Acknowledgements

Saint-Gobain Recherche, France, is gratefully acknowledged for the financial support. Many thanks are given to Céline Cau Dit Coumes (CEA, France) for the constructive suggestions, to Andreas Leemann (Empa, Switzerland), Raül Leiva Muňoz, Nelly Brielles (Saint-Gobain Recherche, France), Wolfgang Kunther (Technical University of Denmark, Denmark) for helpful discussions, to Luigi Brunetti, Bin Ma, Yiru Yan (Empa, Switzerland) for the IC measurements, to Boris Ingold for the SEM sample preparation, to Daniel Rentsch for acquiring the $^{29}Si$ and $^{31}P$ MAS NMR spectra and to Robin Pauer (Empa, Switzerland) for the assisstance with the SEM characterizations.

# Appendices

## A: calcium potassium hydrogen phosphate: $CaK_3H(PO_4)_2$

Pure $CaK_3H(PO_4)_2$ was prepared in duplicate from mixing 28.75 g $KH_2PO_4$ with 14.05 (or 14.96) g KOH and 1.31 g calcium acetate hydrate in 87 mL of water. The samples were equilibrated in closed PE containers for 7 weeks before the suspensions were filtrated and both the aqueous and solid phase were investigated. The results are summarized in Figure A and Table A. The solubility of $CaK_3H(PO_4)_2$ was calculated based on the measured concentrations of Ca, K, phosphate and the pH values using the thermodynamic software GEMS as discussed in 2.2.8 thermodynamic modelling and further detailed in [43].

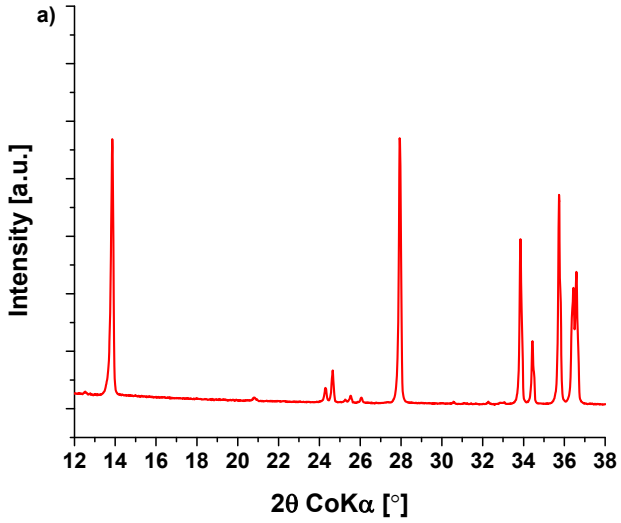

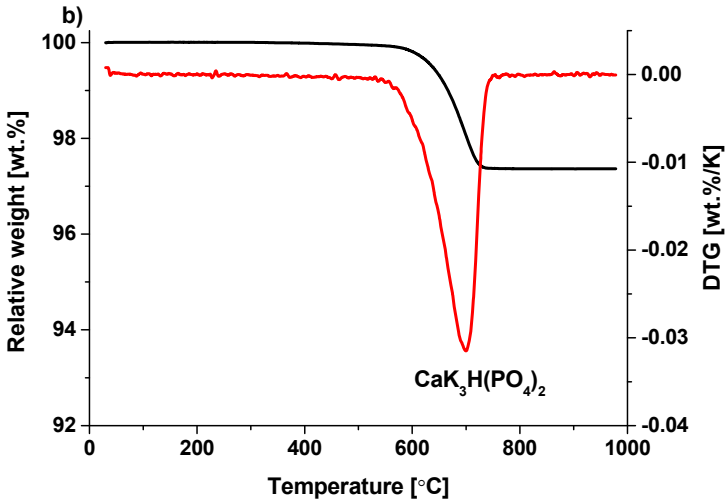


Figure A**:** a) XRD pattern (ICSD code 761248), b) TGA/DTG of $CaK_3H(PO_4)_2$.

Table A: Measured concentrations, pH values and calculated solubility product for $CaHK_3(PO_4)_2 \Leftrightarrow Ca^{2+} + 3K^+ + H^+ + 2PO_4^{3-}$ precipitated from oversaturation at 20°C.

| | K | Ca | $PO_4$ | pH* | Solubility product** |
|---|---|---|---|---|---|
| $CaK_3H(PO_4)_2$ (14.05 g KOH) | 3650 | 0.141 | 1933 | 10.0 | -22.6 |
| $CaK_3H(PO_4)_2$ (14.96 g KOH) | 3640 | 0.197 | 1862 | 10.6 | -22.3 |
| *Mean* | | | | | *-22.4±0.8* |

* pH measured at room temperature and corrected to 20°C. **: $\log K_{SO} = \log (\{Ca^{2+}\}\{K^+\}^3\{H^+\}\{PO_4^{3-}\}^2)$, where {i} indicates the activity of the species i.

The obtained solubility product for $CaHK_3(PO_4)_2 \Leftrightarrow Ca^{2+} + H^+ + 3K^+ + 2PO_4^{3-}$ equals to $K_{so}$ = -22.4±0.8. This value is somewhat lower than the sum of the solubility of brushite ($CaHPO_4 \cdot 2H_2O$, $K_{so}$ = -18.95 [45]) and of $K_3PO_4 \cdot 7H_2O$ ($K_{so}$ = 0.28 [68]), indicating in fact that $CaHK_3(PO_4)_2$ is slightly more stable than brushite and $K_3PO_4 \cdot 7H_2O$ together.

**B: Hydrate assemblages of wollastonite-$KH_2PO_4$ (MgO / $MgCl_2$) suspensions with time**

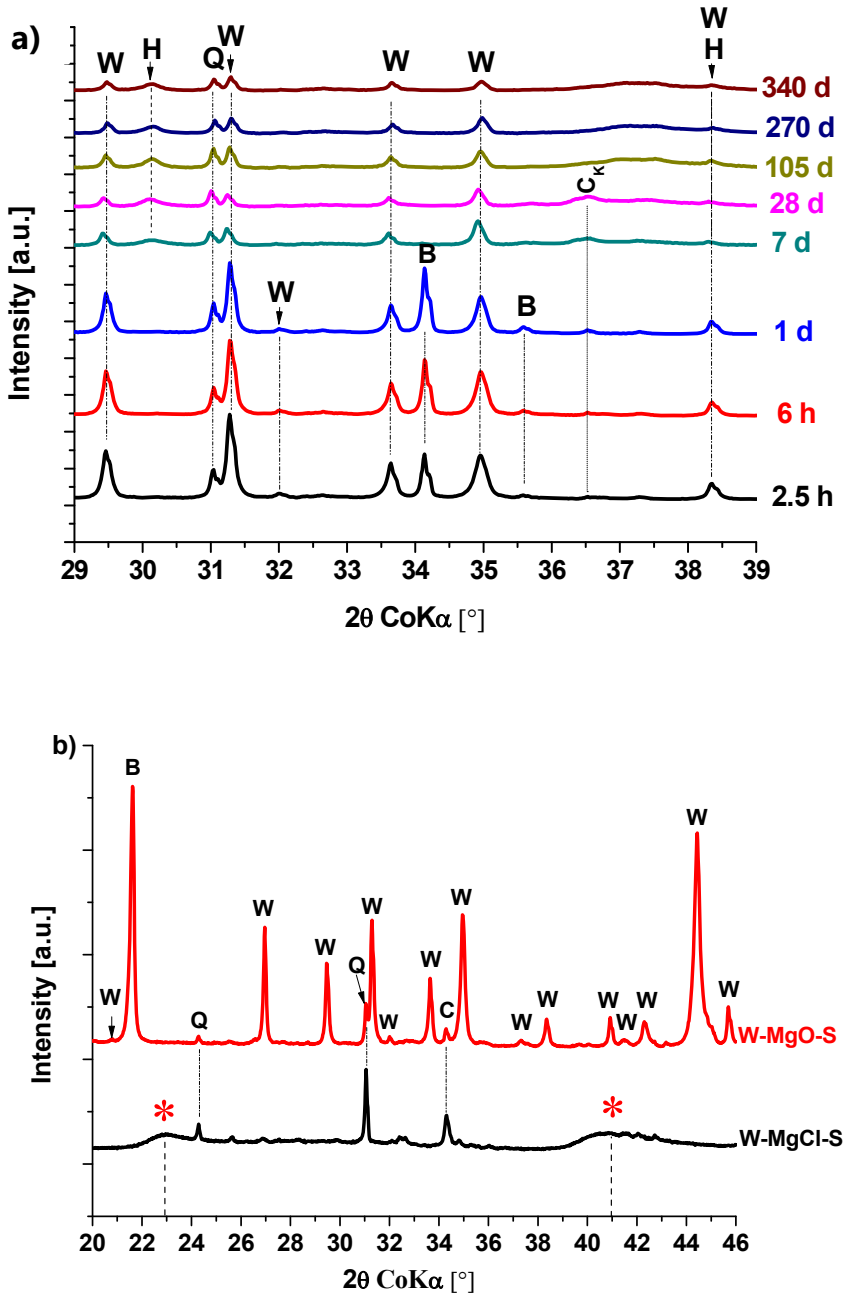


Figure B: XRD patterns of a) wollastonite-$KH_2PO_4$ suspension with time, b) wollastonite – magnesium suspensions (W-MgO-S and W-MgCl-S) with time. $C_K$ = $CaK_3H(PO_4)_2$, B = brushite, H = hydroxyapatite, Q = quartz, W = wollastonite-2M, B = brushite, C = calcite, Q = quartz, W = wollastonite-2M, * = M-S-H.

**C: Hydrate assemblages of the cement suspension with time (2.7-W-S5) with time**

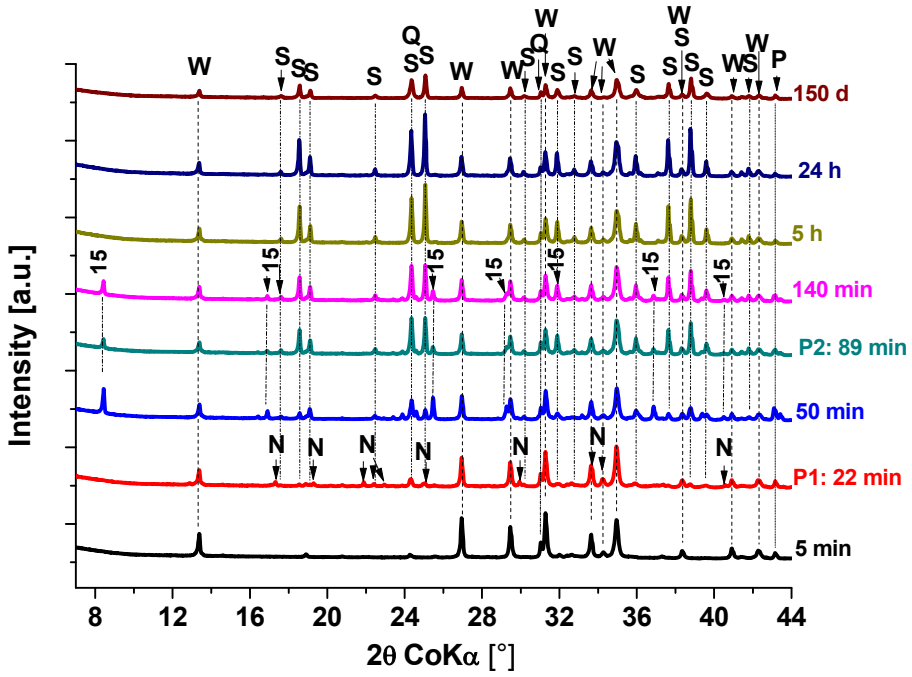


Figure C: XRD patterns of the hydrated cement suspension with wollastonite (2.7-W-S5) with time. N= newberyite, P = periclase, Q = quartz, S = K-struvite, W = wollastonite-2M, 15 = $Mg_2KH(PO_4)_2{\cdot}15H_2O$

## References

[1] A.S.Wagh, Magnesium phosphate ceramics, in: Chemically bonded phosphate ceramics, Elsevier Science 2004, pp. 97-110.

[2] F. Qiao, C.K. Chau, Z. Li, Property evaluation of magnesium phosphate cement mortar as patch repair material, Constr Build Mater, 24 (2010) 695-700.

[3] B. Xu, B. Lothenbach, H. Ma, Properties of fly ash blended magnesium potassium phosphate mortars: Effect of the ratio between fly ash and magnesia, Cem Concr Compos, 90 (2018) 169-177.

[4] H. Lahalle, C. Cau Dit Coumes, A. Mesbah, D. Lambertin, C. Cannes, S. Delpech, S. Gauffinet, Investigation of magnesium phosphate cement hydration in diluted suspension and its retardation by boric acid, Cem Concr Res, 87 (2016) 77-86.

[5] H. Lahalle, C. Cau Dit Coumes, C. Mercier, D. Lambertin, C. Cannes, S. Delpech, S. Gauffinet, Influence of the w/c ratio on the hydration process of a magnesium phosphate cement and on its retardation by boric acid, Cem Concr Res, 109 (2018) 159-174.

[6] B. Xu, F. Winnefeld, J. Kaufmann, B. Lothenbach, Influence of magnesium-to-phosphate ratio and water-to-cement ratio on hydration and properties of magnesium potassium phosphate cements, Cem Concr Res, 123 (2019) 105781.

[7] I. Buj, J. Torras, D. Casellas, M. Rovira, J. de Pablo, Effect of heavy metals and water content on the strength of magnesium phosphate cements, J Hazard Mater, 170 (2009) 345-350.

[8] I. Buj, J. Torras, M. Rovira, J. de Pablo, Leaching behaviour of magnesium phosphate cements containing high quantities of heavy metals, J Hazard Mater, 175 (2010) 789-794.

[9] A.J. Wang, J. Zhang, J.M. Li, A.B. Ma, L.T. Liu, Effect of liquid-to-solid ratios on the properties of magnesium phosphate chemically bonded ceramics, Mat Sci Eng C-Mater, 33 (2013) 2508-2512.

[10] Y. Yu, C. Xu, H.L. Dai, Preparation and characterization of a degradable magnesium phosphate bone cement, Regen Biomater, 3 (2016) 231-237.

[11] F. Qiao, C.K. Chau, Z. Li, Setting and strength development of magnesium phosphate cement paste, Adv Cem Res, 21 (2009) 175-180.

[12] F. Qiao, W. Lin, C.K. Chau, Z.J. Li, Property assessment of magnesium phosphate cement, Key Eng Mater, 400-402 (2008) 115-120.

[13] M. Le Rouzic, T. Chaussadent, L. Stefan, M. Saillio, On the influence of Mg/P ratio on the properties and durability of magnesium potassium phosphate cement pastes, Cem Concr Res, 96 (2017) 27-41.

[14] L.J. Gardner, S.A. Bernal, S.A. Walling, C.L. Corkhill, J.L. Provis, N.C. Hyatt, Characterisation of magnesium potassium phosphate cements blended with fly ash and ground granulated blast furnace slag, Cem Concr Res, 74 (2015) 78-87.

[15] L.J. Gardner, V. Lejeune, C.L. Corkhill, S.A. Bernal, J.L. Provis, M.C. Stennett, N.C. Hyatt, Evolution of phase assemblage of blended magnesium potassium phosphate cement binders at 200° and 1000°C, Adv Appl Ceram, 114 (2015) 386-392.

[16] B. Xu, B. Lothenbach, A. Leemann, F. Winnefeld, Reaction mechanism of magnesium potassium phosphate cement with high magnesium-to-phosphate ratio, Cem Concr Res, 108 (2018) 140-151.

[17] B. Xu, H. Ma, H. Shao, Z. Li, B. Lothenbach, Influence of fly ash on compressive strength and micro-characteristics of magnesium potassium phosphate cement mortars, Cem Concr Res, 99 (2017) 86-94.

[18] L. Mo, L. Lv, M. Deng, J. Qian, Influence of fly ash and metakaolin on the microstructure and compressive strength of magnesium potassium phosphate cement paste, Cem Concr Res, 111 (2018) 116-129.

[19] S.A. Walling, J.L. Provis, Magnesia-based cements: a journey of 150 years, and cements for the future?, Chem Rev, 116 (2016) 4170-4204.

[20] B. Xu, H. Ma, Z. Li, Influence of magnesia-to-phosphate molar ratio on microstructures, mechanical properties and thermal conductivity of magnesium potassium phosphate cement paste with large water-to-solid ratio, Cem Concr Res, 68 (2015) 1-9.

[21] C. Qian, J. Yang, Effect of disodium hydrogen phosphate on hydration and hardening of magnesium potassium phosphate cement, J Mater Civ Eng, 23 (2011) 1405-1411.

[22] Y. Li, T. Shi, B. Chen, Experimental sudy of dipotassium hydrogen phosphate influencing properties of magnesium phosphate cement, J Mater Civ Eng, 28 (2016).

[23] Y.C. Chen, L.X. Wang, P. Song, Q. Wang, Effects of magnesium potassium phosphate cements mixed with silica fume on the solidification and reduction of municipal sludge, Iop Conf Ser-Mat Sci, 167 (2017).

[24] D.D. Zheng, T. Ji, C.Q. Wang, C.J. Sun, X.J. Lin, K.M.A. Hossain, Effect of the combination of fly ash and silica fume on water resistance of Magnesium-Potassium Phosphate Cement, Constr Build Mater, 106 (2016) 415-421.

[25] X.J. Gao, A.L. Zhang, S.X. Li, B.C. Sun, L.C. Zhang, The resistance to high temperature of magnesia phosphate cement paste containing wollastonite, Materials and Structures, 49 (2016) 3423-3434.

[26] A.S. Wagh, S.Y. Jeong, D. Lohan, A. Elizabeth, Chemically bonded phosphate-silicate ceramics (patent), US 6518212B1, US, 2003.

[27] N.M.P. Low, J.J. Beaudoin, Mechanical properties of high performance cement binders reinforced with wollastonite micro-fibres, Cem Concr Res, 22 (1992) 981-989.

[28] N.M.P. Low, J.J. Beaudoin, The effect of wollastonite micro-fibre aspect ratio on reinforcement of Portland cement-based binders, Cem Concr Res, 23 (1993) 1467-1479.

[29] A.M. Soliman, M.L. Nehdi, Effects of shrinkage reducing admixture and wollastonite microfiber on early-age behavior of ultra-high performance concrete, Cem Concr Compos, 46 (2014) 81-89.

[30] W. Ashraf, J. Olek, N. Tian, Multiscale characterization of carbonated wollastonite paste and application of homogenization schemes to predict its effective elastic modulus, Cem Concr Compos, 72 (2016) 284-298.

[31] B. Lothenbach, G. Le Saout, E. Gallucci, K. Scrivener, Influence of limestone on the hydration of Portland cements, Cem Concr Res, 38 (2008) 848-860.

[32] K. Mandel, H. Funke, M. Lindner, S. Gelbrich, L. Kroll, T. Schwarz, Recipe development of low-cost wollastonite-based phosphate cements, Constr Build Mater, 189 (2018) 86-94.

[33] P. Laniesse, C. Cau Dit Coumes, A. Poulesquen, A. Bourchy, A. Mesbah, G. Le Saout, P. Gaveau, Setting and hardening process of a wollastonite-based brushite cement, Cem Concr Res, 106 (2018) 65-76.

[34] H.A. Colorado, Z. Wang, J.-M. Yang, Inorganic phosphate cement fabricated with wollastonite, barium titanate, and phosphoric acid, Cem Concr Compos, 62 (2015) 13-21.

[35] H.A. Colorado, J. Pleitt, C. Hiel, J.M. Yang, H.T. Hahn, C.H. Castano, Wollastonite based-chemically bonded phosphate ceramics with lead oxide contents under gamma irradiation, J Nucl Mater, 425 (2012) 197-204.

[36] W. Ashraf, J. Olek, Carbonation activated binders from pure calcium silicates: reaction kinetics and performance controlling factors, Cem Concr Compos, 93 (2018) 85-98.

[37] B. Lothenbach, P. Durdzinski, K. De Weerdt, Thermogravimetric analysis, in: K. Scrivener, B. Lothenbach (Eds.), A practical guide to microstructural analysis of cementitious materials, CRC Press, Oxford, UK, 2016, pp. 177-212.

[38] F. Winnefeld, B. Lothenbach, Hydration of calcium sulfoaluminate cements — Experimental findings and thermodynamic modelling, Cem Concr Res, 40 (2010) 1239-1247.

[39] B. Lothenbach, Thermodynamic equilibrium calculations in cementitious systems, Mater Struct, 43 (2010) 1413-1433.

[40] D.A. Kulik, T. Wagner, S.V. Dmytrieva, G. Kosakowski, F.F. Hingerl, K.V. Chudnenko, U.R. Berner, GEM-Selektor geochemical modeling package: revised algorithm and GEMS3K numerical kernel for coupled simulation codes, Comput Geosci, 17 (2013) 1-24.

[41] T. Thoenen, W. Hummel, U. Berner, E. Curti, The PSI/Nagra chemical thermodynamic database 12/07, PSI report 14-04, Villigen PSI, Switzerland, 2014.

[42] B. Lothenbach, D.A. Kulik, T. Matschei, M. Balonis, L. Baquerizo, B. Dilnesa, G.D. Miron, R.J. Myers, Cemdata18: A chemical thermodynamic database for hydrated Portland cements and alkali-activated materials, Cem Concr Res, 115 (2019) 472-506.

[43] B. Lothenbach, B. Xu, F. Winnefeld, Thermodynamic data for magnesium (potassium) phosphates, Appl Geochem, 111 (2019) 104450.

[44] E. Bernard, B. Lothenbach, C. Cau Dit Coumes, C. Chlique, A. Dauzères, I. Pochard, Magnesium and calcium silicate hydrates, Part I: Investigation of the possible magnesium incorporation in calcium silicate hydrate (C-S-H) and of the calcium in magnesium silicate hydrate (M-S-H), Appl Geochem, 89 (2018) 229-242.

[45] W.F. Jaynes, P.A. Moore, D.M. Miller, Solubility and ion activity products of calcium phosphate minerals, J Environ Qual, 28 (1999) 530-536.

[46] M. Tung, N. Eidelman, B. Sieck, W. Brown, Octacalcium phosphate solubility product from 4 to 37 °C, J Res Nat Bur Stand, 93 (1988) 613-624.

[47] Q. Liu, Z. Chen, H. Pan, B.W. Darvell, The effect of excess phosphate on the solubility of hydroxyapatite, Ceram Int, 40 (2014) 2751-2761.

[48] K. De Weerdt, M.B. Haha, G. Le Saout, K.O. Kjellsen, H. Justnes, B. Lothenbach, Hydration mechanisms of ternary Portland cements containing limestone powder and fly ash, Cem Concr Res, 41 (2011) 279-291.

[49] J.D. Rimstidt, P.M. Dove, Mineral/solution reaction rates in a mixed flow reactor: wollastonite hydrolysis, Geochim Cosmochim Acta, 50 (1986) 2509-2516.

[50] S.S. Salek, Mineral $CO_2$ sequestration by environmental biotechnological process (Master thesis), National University of Singapore, Singapore, 2015.

[51] W. Ashraf, J. Olek, J. Jain, Microscopic features of non-hydraulic calcium silicate cement paste and mortar, Cem Concr Res, 100 (2017) 361-372.

[52] N. Ma, A.A. Rouff, B.L. Phillips, A $^{31}$P NMR and TG/DSC-FTIR investigation of the influence of initial pH on phosphorus recovery as struvite, ACS Sustainable Chem Eng, 2 (2014) 816-822.

[53] M.A. Aramendía, V. Borau, C. Jiménez, J.M. Marinas, F.J. Romero, J.R. Ruiz, XRD and solid-state NMR study of magnesium oxide–magnesium orthophosphate systems, J Solid State Chem, 135 (1998) 96-102.

[54] J.L. Miquel, L. Facchini, A.P. Legrand, C. Rey, J. Lemaitre, Solid state NMR to study calcium phosphate ceramics, Colloids Surf, 45 (1990) 427-433.

[55] F. Pourpoint, C. Gervais, L. Bonhomme-Coury, T. Azaïs, C. Coelho, F. Mauri, B. Alonso, F. Babonneau, C. Bonhomme, Calcium phosphates and hydroxyapatite: solid-state NMR experiments and first-principles calculations, Appl Magn Reson, 32 (2007) 435–457.

[56] M.R. Hansen, H.J. Jakobsen, J. Skibsted, $^{29}$Si chemical shift anisotropies in calcium silicates from high-field $^{29}$Si MAS NMR spectroscopy, Inorg Chem, 42 (2003) 2368-2377.

[57] J.F. Stebbins, W.R. Panero, J.R. Smyth, D.J. Frost, Forsterite, wadsleyite, and ringwoodite ($Mg_2SiO_4$): $^{29}$Si NMR constraints on structural disorder and effects of paramagnetic impurity ions, Am Mineral, 94 (2009) 626-629.

[58] M.A. Wilson, Chapter 5 - Minerals and their Structure, in: M.A. Wilson (Eds.) NMR Techniques & Applications in Geochemistry & Soil Chemistry, Pergamon, Amsterdam, 1987, pp. 95-138.

[59] E. Bernard, B. Lothenbach, C. Chlique, M. Wyrzykowski, A. Dauzères, I. Pochard, C. Cau-Dit-Coumes, Characterization of magnesium silicate hydrate (M-S-H), Cem Concr Res, 116 (2019) 309-330.

[60] E. L'Hôpital, B. Lothenbach, D.A. Kulik, K. Scrivener, Influence of calcium to silica ratio on aluminium uptake in calcium silicate hydrate, Cem Concr Res, 85 (2016) 111-121.

[61] C. Liu, Y. Huang, W. Shen, J. Cui, Kinetics of hydroxyapatite precipitation at pH 10 to 11, Biomater, 22 (2001) 301-306.

[62] D.R.M. Brew, F.P. Glasser, Synthesis and characterisation of magnesium silicate hydrate gels, Cem Concr Res, 35 (2005) 85-98.

[63] D. Nied, K. Enemark-Rasmussen, E. L'Hôpital, J. Skibsted, B. Lothenbach, Properties of magnesium silicate hydrates (M-S-H), Cem Concr Res, 79 (2016) 323-332.

[64] E. Bernard, A. Dauzères, B. Lothenbach, Magnesium and calcium silicate hydrates, Part II: Mg-exchange at the interface "low-pH" cement and magnesium environment studied in a C-S-H and M-S-H model system, Appl Geochem, 89 (2018) 210-218.

[65] M. Vespa, B. Lothenbach, R. Dähn, T. Huthwelker, E. Wieland, Characterisation of magnesium silicate hydrate phases (M-S-H): A combined approach using synchrotron-based absorption-spectroscopy and ab initio calculations, Cem Concr Res, 109 (2018) 175-183.

[66] A. Bigi, G. Falini, E. Foresti, A. Ripamonti, M. Gazzano, N. Roveri, Magnesium influence on hydroxyapatite crystallization, J Inorg Biochem, 49 (1993) 69-78.

[67] D. Laurencin, N. Almora-Barrios, N.H. de Leeuw, C. Gervais, C. Bonhomme, F. Mauri, W. Chrzanowski, J.C. Knowles, R.J. Newport, A. Wong, Z. Gan, M.E. Smith, Magnesium incorporation into hydroxyapatite, Biomater, 32 (2011) 1826-1837.

[68] T. Scharge, A.G. Muñoz, H.C. Moog, Thermodynamic modelling of high salinary phosphate solutions. I. binary systems, J Chem Thermodyn, 64 (2013) 249-256.